國立交通大學

光電工程研究所

博士論文

# 利用即時側向繞射位置監控及紫外光接續寫入法製作布拉格光纖光柵

# Fiber Bragg Grating Sequential UV-Writing with Real-Time Interferometric Side-Diffraction Position Monitoring

研究生：徐桂珠

指導教授：賴暎杰

中華民國九十六年六月

# 利用即時側向繞射位置監控及紫外光接續寫入法製作布拉格光纖光柵

# Fiber Bragg Grating Sequential UV-Writing with Real-Time Interferometric Side-Diffraction Position Monitoring


研 究 生：徐桂珠　　Student：Kuei-Chu Hsu

指導教授：賴暎杰 博士　　Advisor：Yinchieh Lai


國 立 交 通 大 學

光 電 工 程 研 究 所

博 士 論 文

A Dissertation

Submitted to Department of Photonics and Institute of Electro-Optical Engineering

College of Electrical Engineering and Computer Science

National Chiao Tung University

in Partial Fulfillment of the Requirements

for the Degree of Doctor of Philosophy

in

Electro-Optical Engineering

June 2007

Hsinchu, Taiwan, Republic of China

中華民國九十六年六月

**利用即時側向繞射位置監控及紫外光接續寫入法製作布拉格光纖光柵**

國立交通大學 光電工程研究所

學生：徐桂珠　　指導教授：賴暎杰博士

# 摘要

在本論文中我們首度發展出在紫外光接續寫入布拉格光纖光柵過程中的新型即時光纖位置監控方法，為了即時對準待曝照的次光柵位置，我們使用側向繞射法來偵測另一個單一週期的光纖光柵之相位作為位置的參考點，如此可以較不受量測飄移的影響。

在本研究中我們也仔細校正了紫外光曝光量與光纖引致的折射率變化量之非線性關係圖，經由事先作紫外光處理，可以避免在紫外光量微弱時，因光纖的折射率變化量對紫外光強度呈非線性曲線而造成誤差。我們也發展出使用光強度不相同的新型雙光束干涉法來達到在單次寫入光纖過程中，從而可以保持光纖折射率變化與寫入的紫外光量成正比。

我們也提出一個簡單的方法來達到光纖光柵平均折射率維持定值而折射率調變形狀可加以控制的光纖光柵製造方法。此方法在每一個欲寫入次光柵的位置，將紫外光待曝光量分成前後兩次曝照，而折射率調變的形狀可藉由控制前後寫入兩紫外光的相對相位和強度來調整，如此沿著整個光纖光柵的平均折射率都保持固定值，而局部調整折射率調變的形狀卻可以任意控制。

整體而言，藉著我們發展出的這套光纖光柵製作技術可以建造一個精良的光纖光柵製作平台，從而可以針對不同應用製造出複雜的光纖光柵。

Fiber Bragg Grating Sequential UV-Writing with Real-Time Interferometric Side-Diffraction Position Monitoring

Department of Photonics and the Institute of Electro-Optical Engineering
National Chiao Tung University

Student：Kuei-Chu Hsu Advisor：Prof. Yinchieh Lai

# ABSTRACT

In this dissertation we develop a new real-time fiber position monitoring method for fiber Bragg grating (FBG) sequential UV-writing processes. To real-time accurately align the position of every exposed FBG, a single-period reference fiber grating is probed by applying an interferometric side-diffraction method to measure the grating phase as the position reference, so that the writing process can be less sensitive to the measurement drifts.

During the research we have also calibrated carefully the nonlinear relationship between the UV flux and the induced index change. The pre UV treatment method can avoid the nonlinear index change response regime when the UV flux is low. An improved unequal-intensity UV two-beam interference scheme is proposed and demonstrated to achieve the index response linearization in a single scan.

Finally, a simple method for attaining pure apodization of FBGs has also been proposed. The UV exposure at every exposed location is achieved in two exposure steps and the ac index modulation is adjusted by controlling the superimposed phase and amplitude of the two imprinted UV fringes. The average refractive index is kept constant, and the ac index modulation can be locally and independently changed.

Based on the grating inscription skills, we have developed an excellent grating fabrication platform to produce complex FBGs for various applications.

# ACKNOWLEDGEMENT

我的指導教授，賴暎杰博士，是我在交大的這五年日子裡最重要的人。我會永遠記得賴老師是怎樣期許我往一個真正學者的路邁進。未來的日子裡我未必有他的智慧和能力，但我會學習他的堅持和風範。想起「倚天屠龍記」裡張翠山對恩師張三丰的不勝仰慕欽敬之情，「夫千里之遠，不足以舉其大，千仞之高，不足以極其深。」。這句話也正是我對賴老師崇仰之心的寫照。

很難忘 2005 年在德國作交換學生那個燦爛的夏天。和六位同行的可愛伙伴遊遍德國城市鄉間；在 Jena 小鎮結識親切的陳啟昌老師更是一段很特別的回憶。2006 年到美國亞利桑納大學作為訪問學者的經驗，在各方面的見識都大為增長。亞利桑納大學光學中心裡開放的風氣和優良的學風、學者對學術研究充滿熱忱和全心投入的態度、以及克服一個人在異國生活的種種問題，這些都令我短時間內快速的成長。

交大親友團是我這些年來最大的支柱。許立根學長、陳南光、莊凱評、項維巍、李瑞光及李澄鈴學姊，謝謝你們的專業支持及同門情誼。Kate、森益、至賢、同慶、明芳、鴻章、仁宇、企桓、建舜、晴如、淑惠、鐘响、人豪、柜峰、倩伃、翔榮、鼎鈞、萓蓁、金廠、欣哲、宥涵、佩蓁、宸瑋、宏傑、智明、聖龍、芙涵、室友淑婷，謝謝你們溫暖的友誼。這些年來許多的歡喜和悲傷，沒有你們我絕對撐不下去。特別還要感謝葉李華老師，他作學問的投入態度和創意科學方法，以及對後進不吝鼓勵提攜的熱情，這樣的大師風範，對我的思考和人生觀產生深遠的影響。

謝謝家人無盡的支持。

深深感謝許多人一路走來給我的支持和幫助。我也期許自己，將來一定繼續在專業領域上求進步，以求不辜負大家的期望，也不能辜負自己的期望。

謹將這本論文獻給我在天上的母親。

# CONTENTS

# LIST OF FIGURES

# Chapter 1

# Introduction

## 1.1 Review of Fiber Bragg Grating Devices and Lightwave Applications

The fiber Bragg grating (FBG) research can be dating back to Ken Hill in 1978 [1.1], and during the past few years the research publications in this area still widely appear in international journals and conferences. FBGs are reflective type filters with periodic refractive index modulation running along fiber axis in the fiber core, as shown in Fig. 1.1. Incident wavelengths are reflected when the Bragg condition is satisfied, and otherwise they are transmitted. Owning to all-fiber geometry and low insertion loss, FBGs are critical components in some fiber-optic communication and fiber sensor applications. Today commercial FBG manufacturing technology is already quite matured. The typical grating period is around 535 nm when the reflection center wavelength is located at 1550 nm for optical communication window, and the typical reflectivity is 99.99 %. The center wavelength can be fine-tuned by adding stress on the grating to change its period. Environmental stability was originally a big issue but can be controlled now by suitable annealing process and appropriate package.

FBGs are usually fabricated by imprinting the periodical intensity of UV lights onto the fiber core to induce the periodical refractive index change. The photosensitivity of the core of optical fibers is caused by the fact that the Ge and Si atom bond has the absorption peak around 244 nm. On UV illumination, the bond readily breaks, creating the defect centers that cause refractive index change. Several laser sources with different photosensitive mechanisms are utilized in the literature to

induce periodic refractive index changes inside the fiber. Several fabrication schemes have also been proposed for FBG inscription by forming interference light fringes, including the holographic method and phase mask method. The former is flexible for adjustable Bragg wavelength by changing the two beam interfered angle, while the latter is more insensitive to the environmental variation. In this dissertation, our FBG fabrication process adopts the holographic writing scheme and utilizes 244-nm-UV radiation to induce changes in refractive index.

Besides the optical filtering applications in optic communication, numerous other applications of FBG devices provide a platform for researchers in different optical areas. Several important applications of FBGs are in temperature and strain sensing [1.2], feedback mirror in fiber lasers [1.3], and odd-drop mutiplexers as well as dispersion compensator in optical communication systems [1.4]. The FBG sensors rely on Bragg wavelength shift corresponding to environmental perturbations of strain and temperature. FBGs as feedback mirrors in fiber laser cavities are highly developed recently. Narrow-band FBGs at two ends of rare-earth-doped fibers formed Fabry-Perot laser cavities as DFB (distributed feedback) lasers that support single-longitudinal mode operation. DBR (distributed Bragg reflector) fiber laser is obtained by putting a phase-shifted grating on the rare-earth-doped fibers, so that the grating is treated as a narrow-band transmission filter. Furthermore, the gain-flatten function makes fiber gratings hot devices in fiber amplifiers systems. Many efforts have been made to improve the fiber laser power and output performance by directly writing FBGs on rare-earth-doped fiber and photonic crystal fibers recently [1.5-1.7]. Therefore designing and fabricating state-of-the-art FBGs is promising and very useful in various photonic industries.

## 1.2 Motivation

Advanced fiber gratings have found many applications in various optical areas. Among them, narrow-band FBG devices are important elements for high demanding DWDM and Optical Add/Drop Multiplexer systems as well as in fiber laser systems. Narrow-band FBGs possess long-length and weak refractive index change in optical fibers. Manufacturing such long-length fiber gratings by adopting the phase mask and holographic schemes are limited by the phase mask length or environmental fluctuations respectively.

Our group started the art of FBG design and production in the recent few years and already had achieved some good results in this area [1.8-1.16]. Establishing the easy-realized FBGs technology is our long-term aim of project development. The purpose of this dissertation is to develop a state-of-the-art technique to fabricate narrow-band FBGs with the potential of applying various designs of grating structures. We adopted the side-diffraction method which was originally used for measuring fiber grating index profile and modified the setup to real-time monitor the fiber position during the grating written process. The UV flux and refractive index change profile is further studied to carefully calibrate the photosensitivity relationship curve. Besides, a simple UV exposure method is proposed to achieve pure apodization for fiber Bragg gratings fabricated by sequential UV writing. We believe the fabrication improvement and the calibration results are quite useful in advanced fiber grating fabrication.

To summarize, in this dissertation we have proposed and demonstrated several methods for achieving FBG pure apodization, long-length grating with sequential UV writing, and better linear index response. An advanced FBG fabrication platform is also established based on these methods.

## 1.3 Organization of the Dissertation

This dissertation consists of six chapters. In Chapter 1, the development and application of FBG devices are described. In Chapter 2, the fundamental properties, the photosensitivity of germanium doped silica fibers, and fabrication technology of FBG devices are recounted. In Chapter 3, the proposed real-time side-diffraction position monitoring scheme has been demonstrated to fabricate long-length fiber Bragg gratings. To real-time accurately align the position of every exposed FBG section prior to UV exposure, a single-period reference fiber grating with strong refractive index modulation is probed by applying an interferometric side-diffraction method to measure the grating phase as the position reference. In Chapter 4, the correlation of UV flux and refractive index change of optical fibers is investigated. The pre UV treatment method and unequal two beam interference method are proposed to achieve linear index response of written gratings. In Chapter 5, a simple pure apodization method is proposed. Through the exposure phase and/or time control of multiple UV shots, the ac-index can be adjusted independently with the dc-index kept constant. The conclusions and suggested future works are given in Chapter 6.

## 1.4 References


[1.1] Hill K. O., Fujii Y., Johnson D. C., and Kawasaki B. S., "Photosensitivity in optical waveguides: Application to reflection filter fabrication," Appl. Phys. Lett. **32,** 647-649 (1978).

[1.2] A. D. Kersey, M. A. Davis, H. J. Patrick, M. LeBlanc, K. P. Koo, C. G. Askins, M. A. Putnam, and E. J. Friebele, "Fiber grating sensors," J. Lightwave Technol. **15,** 1442–1450 (1997).

[1.3] J. Archambault, and S. G. Grubb, "Fiber gratings in lasers and amplifiers," J.

Lightwave Technol. **15,** 1378–1384 (1997).

[1.4] C. R. Giles, “Lightwave applications of fiber Bragg gratings,” J. Lightwave Technol. **15,** 1391–1400 (1997).

[1.5] A. Martinez, I. Khrushchev, and I. Bennion, “Direct inscription of Bragg gratings in coated fibers by an infrared femtosecond laser,” Opt. Lett. **31,** 1603-1605 (2006).

[1.6] E. Wikszak, J. Thomas, J. Burghoff, B. Ortac, J. Limpert, S. Nolte, U. Fuchs, and A. Tuennermann, “Erbium fiber laser based on intracore femtosecond-written fiber Bragg grating,” Opt. Lett. **31,** 2390-2392 (2006).

[1.7] J. Albert, A. Schülzgen, V/ L. Temyanko, S. Honkanen, and N. Peyghambarian, “Strong Bragg gratings in phosphate glass single mode fiber,” Appl. Phys. Lett. **89,** 101127 (2006).

[1.8] C.-L. Lee and Y. Lai, “Evolutionary Programming Synthesis of Optimal Long-Period Fiber Grating Filters for EDFA Gain-Flattening,” IEEE Photon. Tech. Lett. **14,** 1557-1559 (2002).

[1.9] L.-G. Sheu, K.-P. Chuang, and Y. Lai, “Fiber Bragg grating dispersion compensator by single-period overlap-step-scan exposure”, IEEE Photon. Tech. Lett. **15,** 1557-1559 (2003).

[1.10] C.-L. Lee and Y. Lai, “Synthesis of long-period fiber gratings using evolutionary programming”, Fiber & Integrated Optics **23,** 249-261 (2004).

[1.11] K.-P. Chuang, L.-G. Sheu, and Y. Lai, “Pure apodized phase-shifted fiber Bragg gratings fabricated by a two-beam interferometer with polarization control”, IEEE Photon. Technol. Lett. **16,** 834-836 (2004).

[1.12] K.-P. Chuang, L.-G. Sheu, and Y. Lai, “Complex fiber grating structures fabricated by sequential writing with polarization control”, Opt. Lett. **29,**

340-342 (2004).

[1.13] C.-L. Lee and Y. Lai, "Optimal dispersionless fiber Bragg grating filter with shorter grating length and smoother dispersion profile", Opt. Comm. **235,** 99-106 (2004).

[1.14] Kuei-Chu Hsu, Lih-Gen Sheu, Kai-Ping Chuang, Shu-Hui Chang and Yinchieh Lai, "Fiber Bragg grating sequential UV-writing method with real-time interferometric side-diffraction position monitoring," Opt. Express **13,** 3795-3801 (2005).

[1.15] Cheng-Ling Lee, Ray-Kuang Lee, Yee-Mou Kao, "Design of multichannel DWDM fiber Bragg grating filters by Lagrange multiplier constrained optimization," Opt. Express **14,** 11002-11011 (2006).

[1.16] Kuei-Chu Hsu, Lih-Gen Sheu, Wei-Wei-Hsiang, and Yinchieh Lai, "Methods of achieving linear index-change response for narrow-band fiber Bragg grating sequential writing," accepted by Opt. Commun.

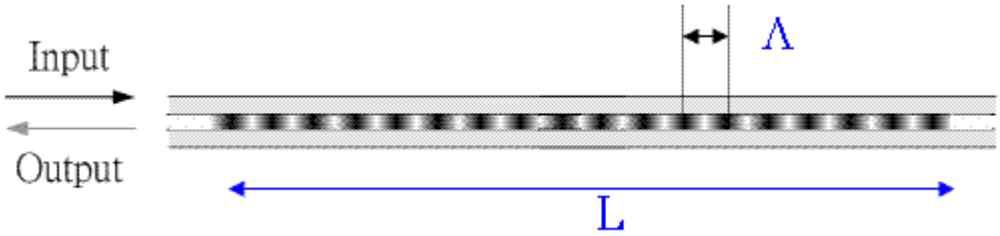


Fig. 1-1 Fiber Bragg grating structure.

# Chapter 2
# Fiber Bragg Grating Model and Fabrication Method

## 2.1 Introduction

The reflection spectrum of the FBG filter and its periodic index profile are Fourier transform pairs in the low index change limit. Getting deeper understanding between the grating structure and its corresponding spectra is useful in designing a desired filter with specific reflection or dispersion purpose. By varying the physical parameters such as index change, length, apodization, period chirp, and fringe tilt, numerous spectral and dispersive characteristics can be achieved. Though many of the mathematical models addressed the relationship between the grating structure and spectra have been developed elsewhere in the literature [2.1-2.3], the simple mathematical model in the first section of this Chapter is described in order to give comprehensive understanding on the FBG optical filtering properties. Since the FBGs are usually photo-imprinted onto the photosensitive fiber, in the second section we state three photosensitivity mechanisms in Germanium-doped optical fibers. Then conventional FBG fabrication methods are briefly demonstrated in the third section.

## 2.2 Theorem of FBG Filters

In the simplest form, FBGs are band-rejection optical filters, and the wavelength selection was governed by the Bragg condition. The mathematical model can be described by the coupled mode equations and solved by the transfer matrix approach.

## 2.2-1 Fundamental Properties of FBG Filters

The fiber Bragg grating is a reflective type filter. The fiber core has spatial refractive index perturbation $\delta_{neff}$ with period $\Lambda$ running along the entire grating length, as shown in the following equation,

$$\delta n_{eff}(z) = \overline{\delta n_{eff}}(z)\{1 + \nu \cos[\frac{2\pi}{\lambda} z + \phi(z)]\}, \quad (2.1)$$

where z is the fiber axis, $\overline{\delta_{neff}}$ is the average effective index, ν is the confinement factor, λ is the wavelength, and $\varphi$ is the grating phase.

Light is reflected when the phase matching condition is satisfied. Setting $\beta_2$ to be the forward propagation constant, $\beta_1$ to be the backward propagation constant, $\lambda_B$ to be the Bragg wavelength, and $n_{eff}$ to be the effective refractive index of the fiber core, then the Bragg condition is described as

$$\beta_2 = \beta_1 - \frac{2\pi}{\lambda}, \quad (2.2)$$

and $\lambda = 2n_{eff}\Lambda$. (2.3)

For optical communication applications, $\lambda_B$ is around 1.55 μm, and hence the grating period is about 535 nm in germanium doped silica fibers.

## 2.2-2 Mathematical Model of FBG Filters

Both the coupled mode equation model and the transfer matrix analysis are commonly used to describe the relationship between the filter spectrum and grating structure [2.2-2.3]. A brief description of coupled mode equation model and transfer matrix approach is given in the following sections.

Consider a fiber grating with spatial index period Λ along the axis coordinate z that causes small perturbations to the mode fields. Two counter-propagating waves in

the optical fiber are denoted as R, and S. Hence the resultant wave coupling can be derived as

$$\begin{aligned} \frac{dR}{dz} &= i\sigma R(z) + i\kappa S(z), \\ \frac{dS}{dz} &= -i\sigma S(z) + i\kappa^* R(z), \end{aligned} \tag{1.3}$$

where

$$\begin{aligned} &\sigma = \frac{2\pi}{\lambda}\overline{\delta n_{eff}}, \\ &and \quad \kappa = \kappa^* = \frac{\pi}{\lambda} v\overline{\delta n_{eff}}. \end{aligned} \tag{1.4}$$

The amplitude reflection coefficient, the reflectivity and the transmission ratio are denoted as ρ, r, t respectively and are defined according to the following equations,

$$\begin{aligned} &\rho = \frac{S(\frac{-L}{2})}{R(\frac{-L}{2})}, \\ &r = |\rho|^2, \\ &and \quad t = 1 - r. \end{aligned} \tag{1.5}$$

The transfer matrix method is a simple way to analyzing complex grating structures by dividing the gratings into small sections with constant period and uniform refractive index modulation. The transform matrix yields the following relationship between the reflected and transmitted waves,

$$\begin{aligned} \begin{bmatrix} \mathrm{u}(L) \\ \mathrm{v}(L) \end{bmatrix} &= T_N \cdot T_{N-1} \cdot \ldots\ldots \cdot T_1 \begin{bmatrix} u(0) \\ v(0) \end{bmatrix} = T \begin{bmatrix} u(0) \\ v(0) \end{bmatrix} \\ &= \begin{bmatrix} T_{11} & T_{12} \\ T_{21} & T_{22} \end{bmatrix} \begin{bmatrix} u(0) \\ v(0) \end{bmatrix}, \end{aligned} \tag{1.6}$$

where u(0) and u(L) represent the input and output forward-propagating waves, v(0) and v(L) are the input and output backward-propagating waves, and L is the length of the grating. The matrix, T, is a function of the refractive index modulation Δn, and the

matrices $T_1$, $T_2$, ….,$T_N$ are governed by the parameters of every grating section. The matrix product of $T_{11}$, $T_{12}$, $T_{21}$, $T_{22}$ forms the final transform matrix. The transmission ratio of the grating can be calculated by

$$t(\delta) = 1/T_{11}, \tag{1.7}$$

where δ is the frequency detuning.

The uniform FBG reflection spectrum possesses apparent side-lobes and thus the FBG refractive index envelopes are usually apodized to be of a gaussian or cosine square shape in order to diminish the side-lobes. The quasi-periodic structure at the long wavelength side originates from the resonance between the abrupt index change of the two ends and can be suppressed by apodizing the index profile. On the other hand, Fabry-Perot resonance between peripheral sections of the grating with apodization cause quasi-periodic structures of the reflection spectrum in shorter wavelengths, which can be reduced by keeping the refractive index constant along the fiber length (pure apodization) [2.4-2.5]. Figure 2.1 depicts the characteristics in the reflection spectra of (a) uniform grating, (b) apodized grating, (c) pure apodized grating.

## 2.3 Photosensitivity in Optical Fibers

The fiber Bragg grating is a kind of phase grating that is produced by imprinting periodic light intensity along the fiber core to establish the periodic index distribution. Due to the photosensitivity of optical fibers, the photo-induced refractive index change forms the required grating distribution. The so-called photosensitivity of germanium-doped silica fibers is caused by the light absorption phenomena of the optical fibers in UV range. The light absorption results in the permanent refractive index change in the core region of optical fibers in the longer wavelengths due to the

Kramers-Kronig relationship [2.6].

Various laser light sources have been used to induce refractive index changes in optical fibers. The commonly used pulse lasers are KrF (248 nm), ArF (193 nm), and Ti-Sapphire (800nm), while the commonly used continuous wave laser is the frequency-doubled Ar-Ion laser (244 nm). Under the intensities of 100-1000 mJ/cm$^2$, the amount of induced refractive index change in germanium doped optical fibers is around $10^{-5}$-$10^{-3}$. Higher index changes can be achieved by hydrogen loading in high pressure [2.7].

## 2.3-1 Photosensitivity Mechanisms in Germanium-Doped Silica Fibers

In the literature [2.6,2.7], the photosensitivity in germanium-doped silica fibers is attributed to three possible mechanisms, the GeE'(color center) model, the stress relief model , and the GeH model. The three mechanisms are recounted in the following sections.

The color center model is based on the principle that the silica fiber core with germanium dopant possesses some defect centers in molecular bonds between Ge and Si atoms and thus has a UV absorption peak. When the UV radiation strongly modifies the defect nature, reconfiguration of molecules locally changes the refractive index of the optical fibers. The higher the germanium concentration, the higher the photosensitivity of the core due to the increase of defect centers [2.8-2.9].

On the other hand, the stress relief model was verified by using AFM to scan the surface of the exposed D-shaped fiber. The induced refractive index change after UV radiation is the result of the relief of frozen internal stress, which produces structural alteration that eventually causes density changes in optical fibers [2.10-2.11].

The third mechanism of the photosensitivity of the core in optical fibers is the formation of GeH after hydrogen-loading [2.12-2.13]. The photosensitivity of Germanium-doped optical fibers is greatly increased in the high-pressure hydrogenation case. The hydrogen reacts with Ge ions and changes the bond structure in the UV region, which in turn locally modifies the refractive index.

### 2.3-2 Photosensitivity in Germanium-Boron Codoped Silicate Fibers

Another breakthrough material development of FBG devices is the invention of germanium-boron codoped silicate fibers [2.6]. The role of boron herein is to reduce the refractive index of the core that is raised by the dopant of germanium. With boron doped, the refractive index difference between the fiber core and cladding area maintains the value that supports single mode propagation, but the more germanium concentration in the core area greatly increases the photosensitivity. The commercially available single mode photosensitive Germanium-boron codoped fibers are usually employed to fabricate fiber gratings with 244-nm UV light.

## 2.4 **Fiber Bragg Grating Fabrication**

In this section, the procedures of fabricating fiber Bragg gratings using the phase mask/two beam schemes with the scanning fiber/light source methods will be introduced. The grating period is controlled by the phase mask period or by the angle of two beams, respectively. Furthermore, the setup to achieve apodization envelope is demonstrated.

## 2.4-1 FBG Fabrication Using Phase-Mask and Two Beam Interference Technique

The commonly used methods to fabricate FBGs are the phase-mask [2.14] and the holographic technique [2.5]. The advantages of the phase mask approach are the easy alignment, low stability requirement, and low coherence laser source requirement. Its drawback, which is the advantage of the holographic approach, is the lack of flexible wavelength tuning capability and the limitation of the grating length. However, the highly environmental requirement is exactly the drawback of the holographic approach.

The phase mask is produced in special glass materials that are transparent to UV lights. The surface is lithographically patterned to form periodic phase distribution. When the light passes through the phase mask, zero order diffraction is highly suppressed, and the two first order diffracted beams can form a periodic intensity distribution with its period half the length of the original phase grating. The fiber is put almost in contact to the mask, so that the periodic intensity pattern can photo-print onto the fiber core to induce the periodic index modulation. To overcome the drawback of grating period tunability limitation, some approaches have used the techniques of applying tension to the optical fiber during writing or changing the writing beam incident angle [2.15].

The holographic (or two beam interference) approach is by dividing the beam into two coherent UV beams and overlap with a mutual angle to form interference pattern. The optical fiber is put in the middle of the illuminated interference pattern. The period can be widely tuned by adjusting the angle of the two interfered beams.

## 2.4-2 Long FBG Fabrication Using Scanning Fiber/Light Source and Sequential Writing Method

DWDM systems as well as single longitudinal mode fiber lasers have high demanding for narrow bandwidth optical filters. For example, the narrow bandwidth FBG is a key element in single longitudinal wavelength laser operation. For weak index gratings, the bandwidth is inversely proportional to grating length. [2.16,2.17] Long-length FBG fabrication is a critical technique, but to actually write a long fiber grating is not easy either in the phase mask or the holographic approach.

To write complex and long-length gratings, some side-writing methods have been demonstrated either by scanning fiber/phase mask approach or by the scanning light source approach. Both methods are valid only with a pulse writing beam or with a shuttered continuous beam in order to control the grating fringe synchronism with the writing interference pattern. The scanning-phase mask writing technique is by scanning fiber constantly by a high precision stage [2.18], and performing the sequential writing by translating the fiber with constant speed relative to the UV fringes, generating many partially overlapping subgratings in sequence to form a long grating. The index profile is accomplished by applying variable dithering, and by adjusting the phase offset of the subgratings. The scanning-light source writing technique is by scanning the UV-beam over a long phase mask in a fixed relative position to the fiber, and the complex profile can be synthesized by designing long appropriate phase mask, by moving the fiber slightly relative to the phase mask, or by second exposure [2.19]. In these methods, a standard He-Ne laser interferometer is utilized to determine the fiber position, and an electronic control by PC is needed to monitor the fiber position and the required jumps to form the complex index profile.

## 2.4-3 Apodization of FBG Index Profile

Uniform gratings with uniform refractive index modulation suffer from considerable side-lobes in the reflection band. FBGs with well-designed apodization profiles can greatly suppress the side-lobes in the reflection spectra and reduce the unwanted ripples in the dispersion curve.

To keep average refractive index the same throughout the length of the grating, pure-apodization method is used. The aim of the method is to maintain the dose of the UV radiation the same throughout the fiber length but the fringe pattern is gradually altering. Conventional method to achieve pure-apodization relies on double UV exposure. The first exposure is to imprint the interference pattern onto the fiber core, followed by second scan to keep the total doze along the entire grating length unchanged [2.20]. The polarization control method was then proposed to inscribe the fiber with complex apodization profiles. In our group, the previous technology of producing apodized fiber grating was accordingly modified and well-developed [2.21-2.22]. Using the shaping function to apodizse the refractive index modulation of the grating and keeping the average refractive index the same along the grating length, the reflection spectrum of the FBGs is perfectly band-rejection and zero side-lobes outside. Figure 2.2(a) shows the diagram of the experimental setup. By rotating the half wave plate, the relative polarization of arms A and B changes, forming the interference pattern of maximum visibility at parallel polarizations and the interference pattern of minimum visibility at orthogonal polarizations. The average refractive index change is constant along the fiber axis due to the overlapped and equal-spaced UV shots that forms constant average UV intensity written onto the fiber, as shown in Fig. 2.2(b).

## 2.3 References


[2.1] T. Erdogan, “Fiber grating spectra,” J. Lightwave Technol. **15,** 1277–1288 (1997).

[2.2] Kogelnik H. and Shank C. W., “Coupled wave theory of distributed feedback lasers,” J. Appl. Phys. **43,** 2327-2335 (1972).

[2.3] Yamada M. and Sakuda. K., “Optical waveguide filters: Synthesis,” J. Opt. Soc. Am. **65,** 804-809 (1975).

[2.4] Mizrahi V. and Sipe J. E., “Optical properties of photosensitive fiber phase gratings,” J Lightwave Technol. **11,** 1513-1517 (1993).

[2.5] Meltz G., Morey W. W., and Glenn W. H., , “Formation of Bragg gratings in optical fibers by transverse holographic method,” Opt. Lett. **14,** 823-825 (1989).

[2.6] Raman Kashyap, “Fiber Bragg Gratings,” Academic Press.

[2.7] Kenneth O. Hill, and Gerald meltz, “Fiber Bragg Grating Technology Fundementals and Overview,” J. Lightwave Technol. **15,** 1263–1276 (1997).

[2.8] T. E. Tasi, G. M. Williams, and E. J. Friebele, “Index structure of fiber Bragg gratings in Ge–SiO2 fibers,” Opt. Lett. **22,** 224–226 (1997).

[2.9] Honso H., Abe Y. Kinser D. L., Weeks R. A., Muta K., and Kawazoe H., “Nature and origin of the 5 eV band in $SiO_2$:$GeO_2$ glasses,” Phys. Rev. B **46,** 445-451 (1995).

[2.10] Douay M., Xie W. X., Taunay T., Bernage P., Niay P., Cordier P., Poumellec B., Dong L., Bayon J. F., Poignant H., and Delevaque E., “Densification involved in the UV based photosensitivity of silica glasses and optical fibers,” J. Lightwave Technol. **15,** 1329–1342 (1997).

[2.11] A I. Gusarov, and D. B. Doyle, “Contribution of photoinduced densification to

refractive-index modulation in Bragg gratings written in Ge-doped dilica fibers," Opt. Lett. **25,** 872–874 (2000).

[2.12] P. J. Lemaire, R. M. Atkins, V. Mizrahi, and W. A. Reed, "High pressure H2 loading as a technique for achieving ultrahigh UV photosensitivity and thermal sensitivity in GeO2 doped optical fibers," Electron. Lett. **29,** 1191–1193 (1993).

[2.13] Atkin R. M., Lemaire P.J., Erdogan T., and Mizrahi V., "Mechanism of enhanced UV photosensitivity via hydrogen loading in germanosilicate glasses," Electron. Lett. **29,** 1234–1235 (1993).

[2.14] K. O. Hill, B. Malo, F. Bilodeau, D. C. Johnson, and J. Albert, "Bragg gratings fabricated in monomode photosensitive optical fiber by UV exposure through a phase mask," Appl. Phys. Lett. **62,** 1035–1037 (1993).

[2.15] K. Nakagawa, Y. Takemura, R. Kunimoto, Y. Mizutani, S. Kimura, Y. Fukuyama, Y. Suzaki, and S. Ejima, "Fabrication of Fiber Gratings with different Bragg wavelengths using a single phase mask," Jpn. J. Appl. Phys. **41,** L599-L601 (2002).

[2.16] J. Albert, K. O. Hill, D. C. Johnson, F. Bilodeau, and M. J. Rooks, "Moire phase masks for automatic pure apodisation of fibre Bragg gratings," Electron. Lett. **32,** 2260–2261 (1996).

[2.17] T. Komukai, K. Tamura, and M. Nakazawa, "An efficient 0.04-nm apodized fiber Bragg grating and its application to narrow-band special filtering," IEEE Photon. Technol. Lett. **9,** 934-936 (1997).

[2.18] Cole M. J., Loh W. H., Laming R. I., Zervas M. N., and Barcelos S., "Moving fiber/phase mask-scanning beam technology for enhanced flexibility in producing fiber gratings with a uniform phase mask," Electron. Lett. **31,** 92–94

(1995).

[2.19] Y. Liu, J. J. Pan, C. Gu, and F. Z. L. Dong, "Novel fiber Bragg grating fabrication method with high-precision phase control," Opt. Eng. **43,** 1916-1922 (2004).

[2.20] A Yang and Y. Lai, "Apodised fiber Bragg gratings fabricated with uniform phase mask using low cost apparatus," Electron. Lett., **36,** 655–657 (2000).

[2.21] Kai-Ping Chuang and Yinchieh Lai, and Lih-Gen Sheu, "Pure Apodized Phase-Shifted Fiber Bragg Gratings Fabricated by a Two-Beam Interferometer With Polarization Control," IEEE Photon. Technol. Lett. **16,** 834-836 (2004).

[2.22] Kai-Ping Chuang and Yinchieh Lai, and Lih-Gen Sheu, "Complex fiber grating structures fabricated by sequential writing with polarization control," Opt. Lett. **29,** 340–342 (2004).

(a)

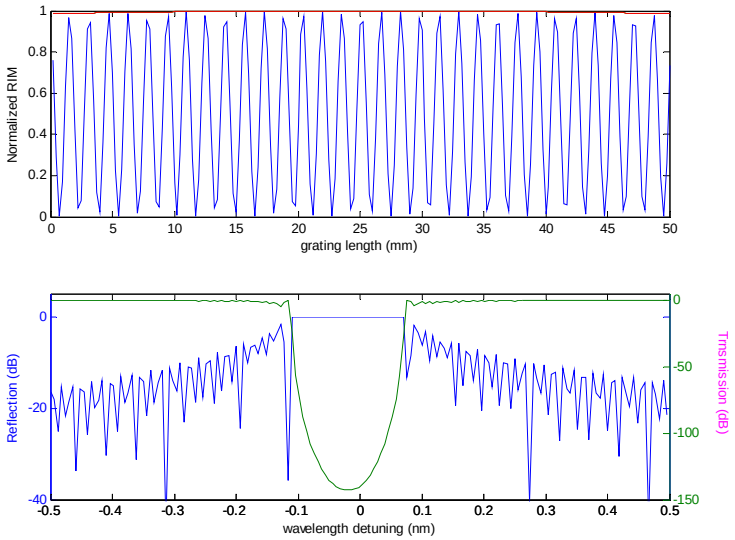
Normalized RIM
grating length (mm)
Reflection (dB)
Transmission (dB)
wavelength detuning (nm)

(b)

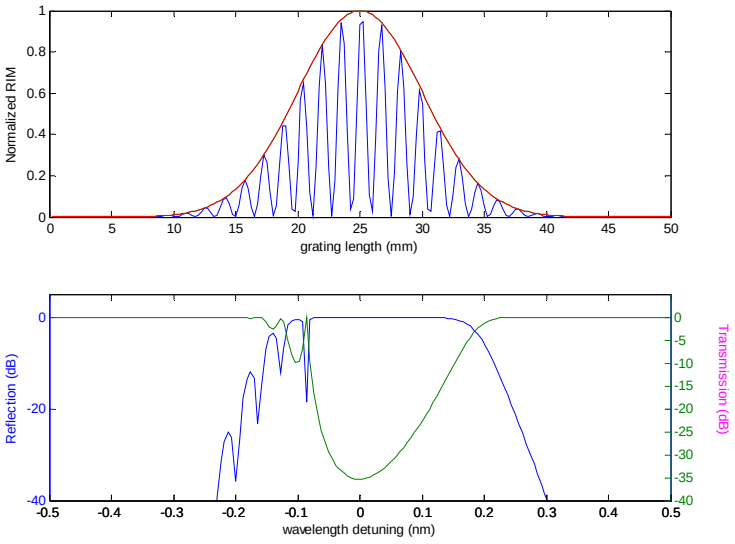
Normalized RIM
grating length (mm)
Reflection (dB)
Transmission (dB)
wavelength detuning (nm)

(c)

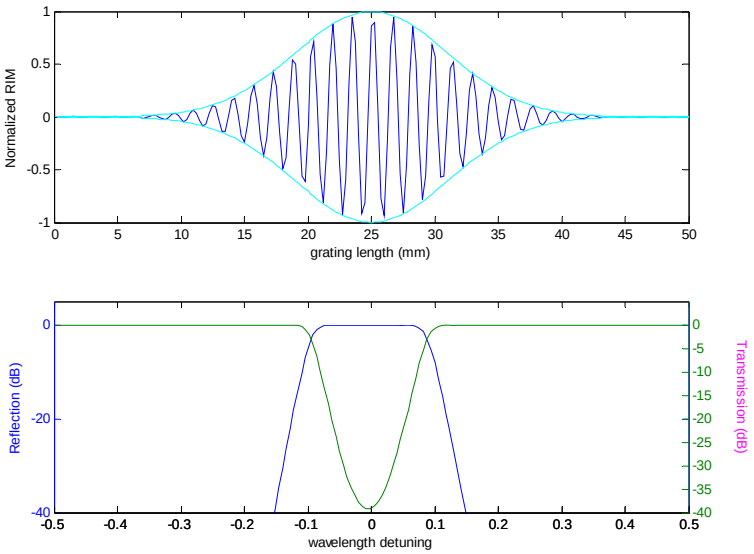


Fig 2.1 (a) Uniform grating index profile and spectrum. RIM: refractive index modulation. (b) Apodized grating index profile and spectrum. (c) Pure apodized grating index profile and spectrum.

(a)

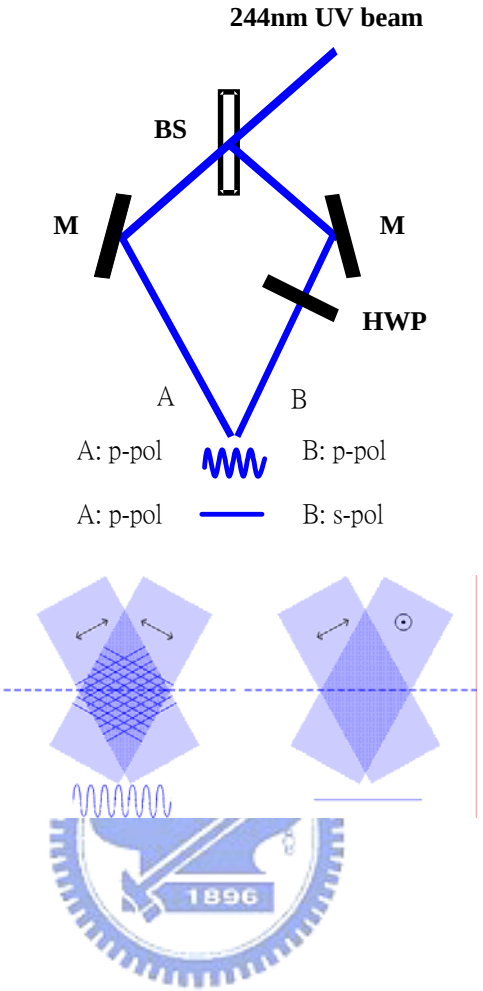


(b)

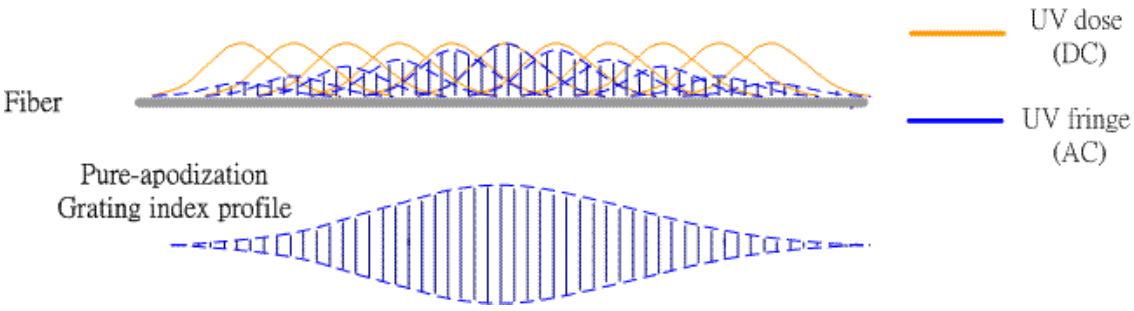


Fig 2.2 (a) Pure apodization setup. M: Mirror, HWP: half wave plate, BS: beam splitter, A: arm A, B: arm B. (b) Sequential writing with constant average refractive index along the entire grating length.

# Chapter 3
# Fiber Bragg Grating Fabrication by Interferometric Side-Diffraction Position Monitoring Scheme

## 3.1 Narrow Band FBGs

Advanced fiber Bragg gratings (FBGs) with complex grating structures of arbitrary phase shifts and refractive index profiles have been continuously attractive for many optical communication applications, including narrow-band FBG OADMs, dispersion compensators, sensors, phase-shifted DFB fiber lasers and pulse repetition-rate multiplication [3.1-3.5]. Several procedures that can realize long and complex FBG structures have recently been developed, such as the moving-fiber-scanning-beam technique [3.6] and the sequential writing techniques [3.7]. In these methods, a conventional laser interferometer is typically utilized to monitor the fiber/UV-beam position during the writing process. However, accumulative position reading errors due to interferometer drift and inaccurate grating period estimation have caused significant difficulties on the fabrication of long-length fiber Bragg gratings.

To overcome some of these difficulties, we utilize the side-diffraction interference method [3.8] for real-time monitoring the fiber position accurately during the sequential writing process [3.9-3.11]. The side-diffraction interference technique was originally developed for measuring the variation of the grating period and the refractive-index modulation profile of the exposed FBGs [3.8]. In the literature it has

also been suggested that the method can be used as a position control scheme [3.12]. However, we believe our work is the first experimental report on actually using the method for real-time position monitoring during the FBG fabrication process. By directly measuring the grating phase, we can connect adjacent grating sections with accurate phase alignment.

## 3.2 Interferometric Side Diffraction Method

The purpose of developing interferometric side-diffraction technique was to measure the refractive-index modulation profiles of FBG devices [3.8-3.12]. In the literature, the interferometric side-diffraction technique was first proposed by Fonjallaz et. al. Then Fouad El-Diasty et. al. modified the experimental setup to preciously obtain index modulation and periodicity of FBGs.

There are numerous methods for measuring the fiber grating structure, such as optical low-coherence reflectometry, heat scanning method, side Rayleigh scattering profiling, and optical low-coherence reflectometry with scanning local heating, side-diffraction, and side-diffraction with local heating [3.13-3.18]. They are either limited in strong grating measurements or limited in short grating length. The interferometric side-diffraction method is the most precise measurement method regardless of the fiber grating length and index modulation. The advantage of the setup is due to the use of the visibility of the two beam interference pattern, so that the weaker grating can be measured by tuning the intensity ratio of the two interfered beams, and by use of the translation stage to scan entire fiber grating length. Thus, a weak index modulation profile can be determined regardless of the weak intensity of diffraction beam. According to the equation derived by Fouad El-Diasty et. al., the index modulation of the local grating section is proportional to the first order Bragg

diffraction intensity.

We have built an interferometric side-diffraction setup and the interference pattern is captured by a CCD camera which is automatically controlled by a computer to do the whole data processing. In our side-diffraction setup, the fiber is clamped on the translation stage with the position monitoring resolution of sub-μm by an Agilent 5519A He-Ne laser interferometer, as shown in Fig. 3.1. A 35-mW high power He-Ne laser beam of 3-mm-diameter is divided into two beams: one is the probe beam and the other is the reference beam. The probe beam is focused onto the fiber grating under test with a spherical lens of 20-cm focal length. The first-order Bragg diffraction of the probe beam is generated under the phase-matching Bragg condition. This diffracted probe beam and the reference beam are combined at the beam combiner to form an interference pattern. A 440×480 monochrome CCD camera with a pixel width of 7.15-μm is utilized to record the interference pattern produced by the two beams. The CCD is proven to have linear response to He-Ne laser power and its S/N ratio is 50 dB. The refractive index profile is obtained by analyzing the visibility of the interference pattern with Fourier transform along the whole grating. With the use of the polarization beam splitter, the power ratio of the two beams can be controlled by adjusting the angles of the waveplates to get good visibility contrast even in the weak grating case. According to Ref. [3.8], the refractive index variation is directly proportional to the amplitude of the first order diffraction beam. In our setup, the interference pattern is taken Fourier transform to get the amplitude of the beating frequency between the reference beam and the diffractive beam. Let the intensity of reference beam be $I_r$, and the intensity of first order diffraction beam be $I_d$, the interference pattern distribution along x axis is I(x), and the refraction index change is Δn, then

$$I(x) = I_r + I_d + 2\sqrt{(I_r I_d)}\cos(2\pi fx), \tag{3.1}$$

and $\Delta n = c\sqrt{I_d}$ , (3.2)

where f is the spatial frequency of the interference pattern, and c is constant. In our experimental setup, the minimum detectable refractive index variation of the grating is around $5\times10^{-6}$, depending on the probe laser power and the optimized intensity ratio of the divided two laser beams.

## 3.3 Fiber Bragg Grating Fabrication by Interferometric Side-Diffraction Position Monitoring

In this section, two real-time side-diffraction position monitoring schemes for fabricating long fiber Bragg gratings are investigated. In the first scheme, the side diffraction position monitoring method that probes the just-exposed grating section has been developed to fabricate single-period fiber Bragg gratings. Because the grating phase of the just-exposed grating section is still affected by the later exposures due to the strongly overlap exposure scheme we use, and because it is difficult to form a clear interference pattern for the side-diffraction measurement when the refractive index modulation is lower than $3.0 \times 10^{-5}$, this simple method is only suitable for fabricating single-period fiber FBGs with reasonable strength index modulation. The second scheme employs a reference fiber Bragg grating with a uniform strong refractive index profile fabricated by using the first scheme. The reference grating is placed in parallel to the exposure fiber on the moving stage. Prior to the UV exposure of every FBG section, the reference fiber grating is probed with the side-diffraction method to determine the grating phase as the reference. The measured value can then provide an accurate fiber position reference during the fabrication process. The second scheme shares the same advantage with the first scheme that the accumulative position

measurement errors during the long fiber scan can be avoided. Moreover, it also has the following additional advantages. First of all, long FBGs with weak index modulation can be fabricated. The first scheme fails to do this because the resolution of our side-diffraction monitoring scheme is limited to $3.0 \times 10^{-5}$ refractive index modulation. Secondly, phase shifts along the fiber grating can be easily inserted. The first scheme fails to do this because with the insertion of phase shifts, the grating phase of the just-exposed section will still not reach the final value due to the strongly-overlapped exposure method we use [3.9-3.11]. Thirdly, the required reference FBG can be fabricated by a similar setup (the first scheme) or by different methods (i.e., the phase mask method). In principle, the second scheme will be capable of fabricating arbitrary FBG refractive index modulation profiles with arbitrary grating phase shifts. Details of the experimental setups and the achieved results for the proposed schemes will be presented during the following sections.

### 3.3.1 Fiber Bragg Grating Fabrication by Interferometric Side-Diffraction Position Monitoring with Exposed Fiber Section

Our first real-time side-diffraction position monitoring method is by probing the just-exposed fiber grating section. Figure 3.2(a) shows the schematic diagram. A 35-mW single-polarization He-Ne laser beam is expanded with two spherical lenses to achieve a final beam diameter of roughly 3 mm. It is then divided into two probe beams A and B with a polarization beam splitter. The function of the first half-wave plate is to control the intensity ratio of these two divided beams. The second half-wave plate rotates the polarization of the probe beam B relative to the probe beam A. Probe beam A is then focused onto the exposed fiber with a spherical lens of 20-cm focal length. The first-order Bragg diffraction of probe beam A is generated under the

phase-matching Bragg condition $\sin\theta_1 = n_B \cdot \lambda / \lambda_B$, where $\theta_1$ is the input angle of the probe beam in air, $n_B$ is the effective index of the exposed fiber at the Bragg wavelength $\lambda_B$, and $\lambda$ is the wavelength of the probe beam. Probe beam B and diffracted probe beam A are combined at the beam combiner with an interference angle of $\theta_2$. A 440×480 monochrome CCD camera with a pixel width of 7.15-μm is utilized to record the interference pattern produced by probe beams A and B. The visibility of the interference pattern can be optimized by adjusting the two half-wave plates. A frequency-doubled argon-ion laser launches a CW 244-nm single-polarization ultra-violet (UV) beam into a two-beam interferometer. Exposure of the Gaussian-shaped UV fringe with its $1/e^2$ width about 6.5 mm forms a periodic UV intensity pattern onto the exposed fiber to induce a single FBG section. The long fiber Bragg grating is achieved by connecting many strongly-overlapped, equally-spaced, Gaussian-shaped FBG sections with accurate grating phase alignment. A half-wave plate is placed in one path of the two interfering beams to obtain pure apodization (flat DC-index modulation) for the final FBG [3.19]. The translation stage comprises of a linear motor stage and a piezoelectric translator (PZT) stage with sub-nm position resolution. The accurate alignment of the fiber position is achieved by shifting the translation stage by a given distance and then iteratively fine-tuning the PZT stage according to the grating phase measurement of the just-exposed grating section. In our preliminary experimental setup, the position monitoring accuracy of the whole system is better than 4 nm, but the accuracy of the position-seeking feedback control loop is only set to be around 5 nm (1% of the grating period) in order to reduce the required position-seeking time. The measurement accuracy we have readily achieved is two-fold better than the estimated accuracy in Ref.[3.8]. The intensity of the first-order diffracted probe beam A is denoted as $I_A$, and the intensity of the probe beam B is

assumed to be $I_B$. The intensity distribution of the interference fringe on the CCD along the x-axis, which is perpendicular to the bisector of the two interfering beams, is given by

$$I_{\text{int}} = I_A + I_B + 2\sqrt{I_A I_B} \cdot \cos[kx \cdot 2\sin(\frac{\theta_2}{2}) + \delta], \tag{3.3}$$

where $k=2\pi/\lambda$ is the wave vector, $\theta_2$ is the interfering angle and $\delta$ is the phase difference between the two interfering beams. The phase difference $\delta$ contains two contributions,

$$\delta = \delta_{grating} + \delta_{path\ difference}, \tag{3.4}$$

where $\delta_{\text{grating}}$ is the phase change of the diffracted probe beam A caused by the fiber grating, and $\delta_{\text{path difference}}$ is the phase change caused by the optical path difference between two probe beams. Since $\delta_{\text{path difference}}$ is constant during the scan, the grating phase change can be inferred from monitoring the phase difference $\delta$. The interference pattern $I_{\text{int}}$ is processed by the Fourier transform to obtain the corresponding spatial frequency spectrum. The spectrum is then filtered to keep only the positive frequency part and is inverse-Fourier-transformed back to the original domain. The phase $\delta$ can then be identified by taking the arg of the processed data. Figure 3.2(b), Fig. 3.3(a) and Fig. 3.3(b) show the typically resulted periodic pattern captured by the CCD camera (grey solid line), the pattern after the filtering + taking-real-part procedure (grey dotted line) and the obtained phase distribution by taking the arg of the filtered data (bold solid line). For producing single period FBGs, the PZT stage is fine tuned until the just-exposed fiber grating phase distribution obtained in this step is the same as that of last step. The UV-beam shutter is then turned on for writing the present FBG section with a given time duration. In practice, the whole algorithm is implemented with the LabVIEW software for automatically controlling the whole exposure process.

As an example, this side diffraction position monitoring method that probes the

just-exposed section has been employed for preparing a single-period fiber grating with strong index-modulation. The fiber used is the photosensitive fiber (Fibercore PS1500) after 1,900-psi hydrogen loading at room temperature for several days. The Gaussian-shaped UV fringe has its $1/e^2$ width about 6.5 mm and the fiber scan step is about 1mm. The final FBG is produced after a 80-section sequential writing to reach a total grating length about 80 mm. The same side-diffraction method [3.8] is applied to measure the whole refractive index modulation profile of the fabricated fiber grating. Figure 3.4 shows the measured result. One can see that the fabricated fiber grating profile is substantially uniform. The optical reflection spectrum in the inset of Fig. 3.4 shows that the Bragg wavelength is 1.546 μm and there should be no obvious phase errors. Such a FBG will be used as the reference grating for the scheme in next section.

### 3.3.2 Fiber Bragg Grating Fabrication by Interferometric Side-Diffraction Position Monitoring with Reference Fiber Grating

In the second scheme, the experimental setup includes a reference fiber grating and an exposure fiber which are clamped in parallel on the same moving stage. Figure 3.5(a) depicts the schematic diagram of the system. The reference grating with a strong and uniform refractive index modulation is prepared in advance with the first scheme. The reference fiber grating under probe is adequately uniform and has a sinusoidal index modulation profile n(x) along its fiber axial direction as

$$n(x) = n_0 + \Delta n \cdot \cos\left(\frac{2\pi x}{\Lambda} + \phi(x)\right), \tag{3.5}$$

where $n_0$ is the average refractive index, $\Delta n$ is the amplitude of refractive index modulation, $\Lambda$ is the grating period, and $\phi(x)$ describes spatial grating phase. The

UV-generated interference period is fine tuned to match the reference fiber grating period, even though this restriction can be relaxed since it will only cause a center-wavelength shift. The accurate alignment of the fiber position is achieved by shifting the translation stage by a given distance and then iteratively fine-tuning the PZT stage according to the reference grating phase measurement. The UV-beam shutter is then turned on for writing the present FBG section with a given time duration. Figure 3.5(b) reveals the flow chart of the whole operation algorithm. In principle, this method should be able to fabricate long fiber Bragg gratings even when the index-modulation is small and with the option for easy insertion of arbitrary phase shifts. We have verified the feasibility of the proposed method by two examples. The first example is to fabricate a narrowband, Gaussion apodized FBG with a constant DC refractive index modulation along the whole grating, as shown in Fig. 3.6(a). The reference grating with uniform and strong refractive index modulation is probed to identify the related grating phase information. The Gaussian-shaped UV fringe has its $1/e^2$ width about 6.5 mm and the fiber scan step is about 1.2 mm. The final FBG is produced after a 58-section sequential writing to reach a total grating length about 70 mm. Before the UV writing process, a DC pre-UV treating process is applied to avoid the nonlinear regime when the exposure UV flux is small [3.20]. Figure 3.7(a) shows the reflection and transmission spectra of the exposed FBG. The reflection spectrum has a relatively flat top with the sidelobe level below -20 dB. The 3-dB bandwidth of the reflection spectrum is only 0.07 nm. The peak refractive index modulation is estimated to be $2.5\times10^{-5}$ for this 70-mm-long Gaussian apodized FBG, determined by simulation-fitting. This example demonstrates the feasibility for fabricating long fiber Bragg gratings without noticeable phase errors, even when the written index modulation is below the threshold for reliable side-diffraction measurement.

The second example is to fabricate a 40-mm-long, single π-phase-shifted Gaussion apodized FBG with a constant DC refractive-index modulation, as shown in Fig. 3.6(b). The scan step during the exposure is about 0.6 mm and the final FBG is achieved by connecting 70 FBG sections. A π phase shift is inserted into the center of the exposure fiber grating during the fabrication process. Figure 3.7(b) shows the reflection and transmission spectrum of the exposure fiber. As expected, there is a narrow transmission peak within the stop-band due to the resonance caused by the π-phase-shift. This simple example demonstrates the feasibility of fabricating phase-shifted FBGs with the new scheme.

## 3.4 Summary

In conclusion, we have proposed and demonstrated a real-time fiber position monitoring method for sequential UV-writing processes by using the interferometric side-diffraction technique. This new method (the second scheme) is capable of fabricating long FBGs with weak index modulation and easily to insert phase shifts along the fiber grating. Furthermore, the required reference FBG can be fabricated by a similar setup (the first scheme) or by different methods (i.e., the phase mask method). Several preliminary examples have been experimentally demonstrated for proving the feasibility of the new method. Hopefully this new method is promising for increasing the accuracy and the ease of fabricating complicated long FBG devices.

## 3.5 References


[3.1] T. Komukai, K. Tamura, and M. Nakazawa, “An efficient 0.04-nm apodized fiber Bragg grating and its application to narrow-band spectral filtering,” IEEE Photon. Technol. Lett. **9,** 934–936 (1997).

[3.2] J. T. Kringlebotn, J. L. Archambaut, L. Reekie, and D. N. Payne, “Er3+:Yb3+-codoped fiber distributed-feedback laser,” Opt. Lett. **19,** 2101-2103 (1994).

[3.3] Junfeng Jiang, Tiegen Liu, Yimo Zhang, Lina Liu, Ying Zha, Fan Zhang, Yunxin Wang, and Pin Long, “Parallel demodulation system and signal-processing method for extrinsic Fabry–Perot interferometer and fiber Bragg grating sensors ,“Opt. Lett. **30,** 604-606 (2005).

[3.4] Naum K. Berger, Boris Levit, Shimie Atkins, and Baruch Fischer, “Repetition-rate multiplication of optical pulses using uniform fiber Bragg gratings,” Opt. Commun. **221,** 331-335 (2003).

[3.5] Xu Wang, Koji Matsushima, Ken-ichi Kitayama, Akihiko Nishiki, Naoya Wada and Fumito Kubota, “High-performance optical code generation and recognition by use of a 511-chip, 640-Gchip_s phase-shifted superstructured fiber Bragg grating,” Opt. Lett. **30,** 355-357 (2005).

[3.6] M. J. Cole, W. H. Loh, R. I. Laming, M. N. Zervas and S. Barcelos, “Moving fiber/phase mask-scanning beam technique for enhanced flexibility in producing fibre gratings with uniform phase mask,” Elect. Lett. **31,** 1488-1490 (1995).

[3.7] Petermann, B. Sahlgren, S. Helmfrid, A. T. Friberg, and P.-Y. Fonjallaz, “Fabrication of advanced fiber Bragg gratings by use of sequential writing with a continuous-wave ultraviolet laser source,” Appl. Opt. **41,** 1051-1056 (2002).

[3.8] F. El-Diasty, A. Heaney, and T. Erdogan, “Analysis of fiber Bragg gratings by a side-diffraction interference technique,” Appl. Opt. **40,** 890-896 (2001).

[3.9] K.-P. Chuang, I.–L. Wu and Yinchieh Lai, “Interferometric side-diffraction position monitoring technique for writing long fiber Bragg gratings,” CLEO/IQEC, CThM6 (2004).

[3.10] Kuei-Chu Hsu, Lih-Gen Sheu, Kai-Ping Chuang, Shu-Hui Chang and Yinchieh Lai, “Fiber Bragg grating sequential UV-writing method with real-time interferometric side-diffraction position monitoring,” Opt. Express **13,** 3795-3801 (2005).

[3.11] Kuei-Chu Hsu, Lih-Gen Sheu, and Yinchieh Lai, “Fabrication of Fiber Bragg Gratings by Sequential UV-Writing with Real-Time Interferometric Side-Diffraction Position Monitoring”, ECOC2005, We4.P.132.

[3.12] Mattias Åslund, John Canning, Leon Poladian, and C. Martijn de Sterke, “Novel characterization technique with 0.5 ppm spatial accuracy of fringe period in Bragg gratings,” Opt. Express **11,** 838-842 (2003).

[3.13] N. Roussel, S. Magne, C. Martinez, and P. Ferdinand, “Measurement of index modulation along fiber Bragg gratings by side scattering and local heating techniques,” Opt. Fiber Technol. **5,** 119–132 (1999).

[3.14] P. A. Krug, R. Stolte, and R. Ulrich, “Measurement of index modulation along an optical fiber Bragg grating,” Opt. Lett. **20,** 1767–1769 (1995).

[3.15] W. Margulis, I. G. Carvalho, and P. M. Gouvea, “Heat scan: a simple technique to study gratings in fiber,” Opt. Lett. **18,** 1016–1018 (1993).

[3.16] P. Lambelet, P. Y. Fonjallaz, H. G. Limberger, R. P. Salathe, Ch. Zimmer, and H. H. Gilgen, “Bragg grating characterization by optical low-coherence reflectometry,” IEEE Photon. Technol. Lett. **5,** 565–567 (1993).

[3.17] B. L. Danielson and C. D. Whittenberg, “Guided-wave reflectometry with micrometer resolution,” Appl. Opt. **26,** 2836– 2842 (1987).

[3.18] K. Takada, I. Yokohama, K. Chida, and J. Noda, “New measurement system for fault location in optical waveguide devices based on an interferometric technique,” Appl. Opt. **26,** 1603–1606 (1987).

[3.19] K.-P. Chuang, Y. Lai, and L.-G. Sheu, “Pure apodized phase-shifted fiber Bragg gratings fabricated by a two-beam interferometer with polarization control,” IEEE Photon. Technol. Lett. **16,** 834-836 (2004).

[3.20] B.-O. Guan, H.-Y. Tam, X.-M. Tao, and X.-Y. Dong, “Highly stable fiber Bragg gratings written in hydrogen-loaded fiber,” IEEE Photon. Technol. Lett. **12,** 1349-1351 (2000).

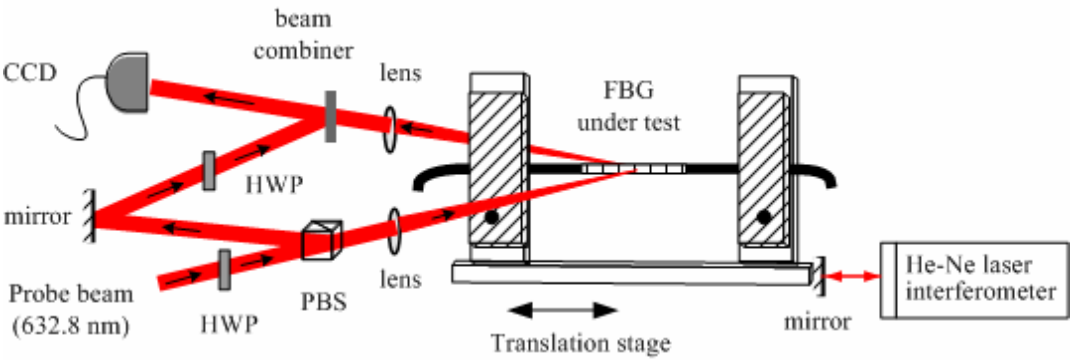


Figure 3.1. Experimental setup of side-diffraction method. HWP: half wave plate, PBS: polarization beam splitter.

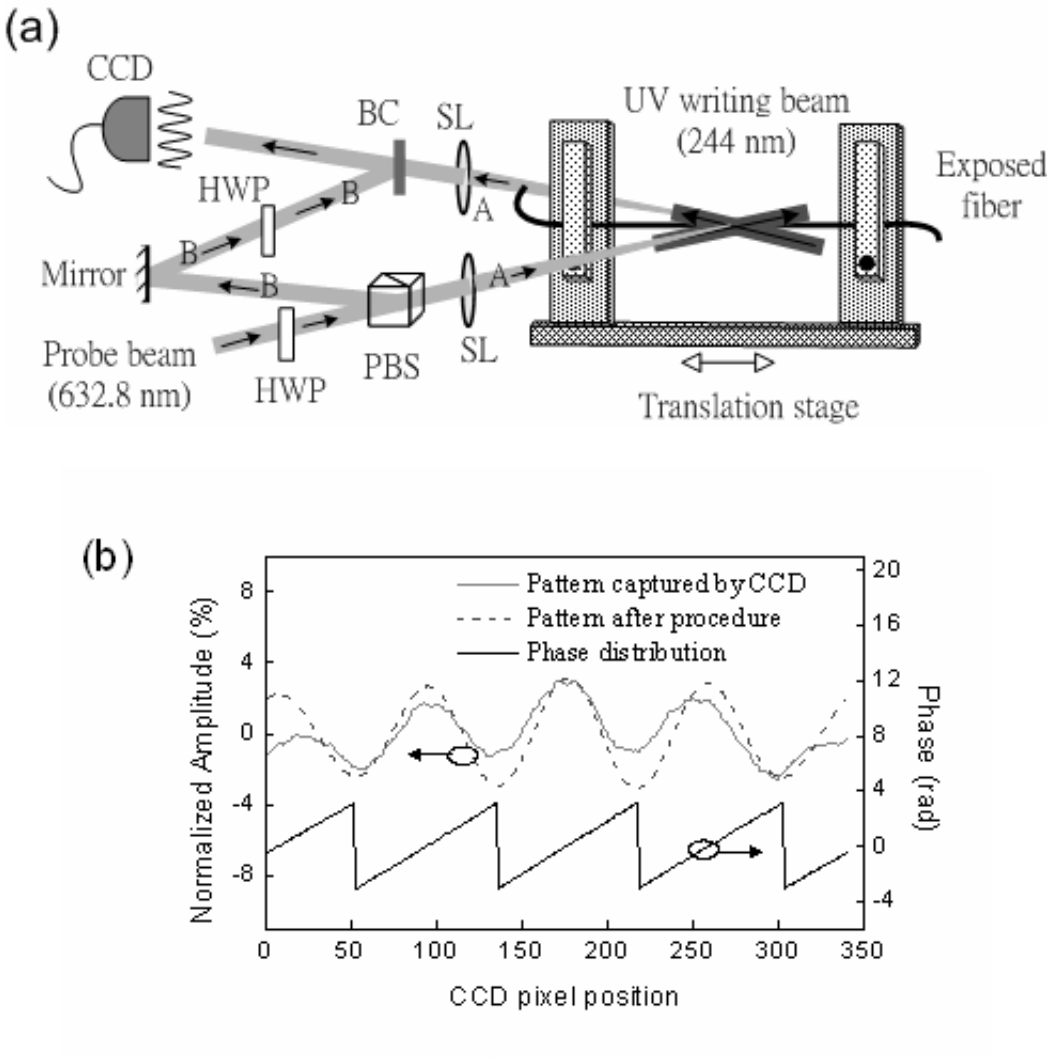


Fig. 3.2. (a) Real-time side-diffraction position monitoring setup by probing the just-exposed section. SL: spherical lens; BC: beam combiner; PBS: polarization beam splitter; HWP: half wave plate. (b) Typical interference pattern captured by CCD, the pattern after procedure (filtering+taking-real-part) and the calculated phase distribution.

(a)

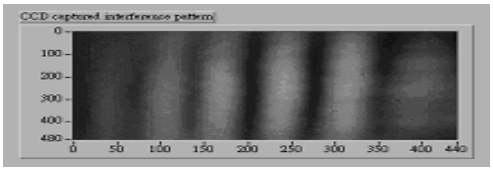


(b)

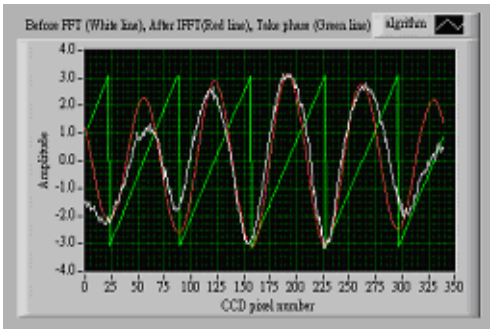


Fig. 3.3. (a) Interference pattern captured by CCD. (b) White line: Original pattern, Red line: Pattern after , procedure, Green line: Periodic phase.

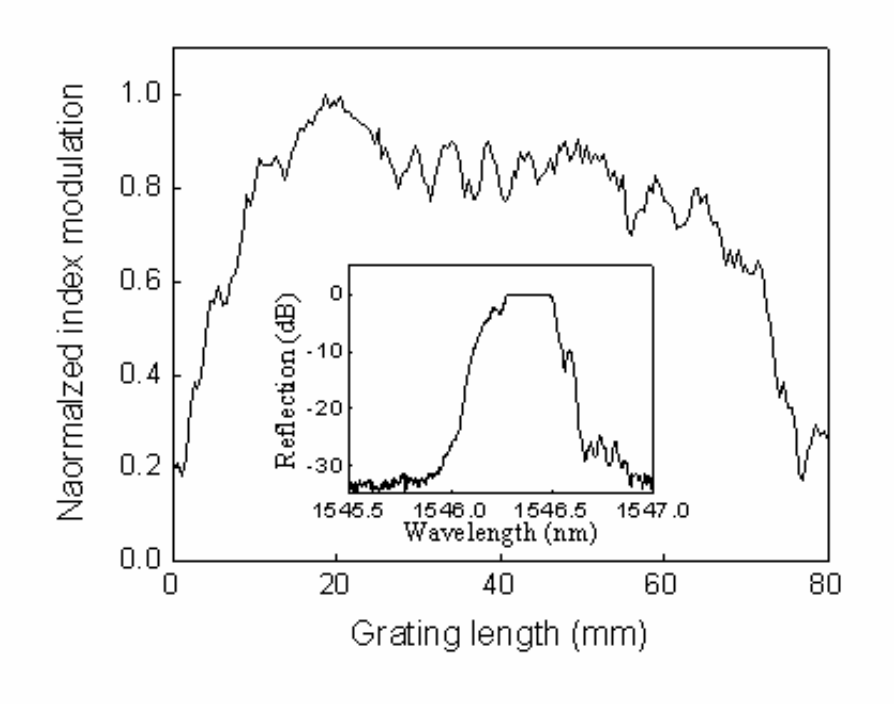


Fig. 3.4. Refractive index profile and Bragg wavelength of a uniform fiber grating

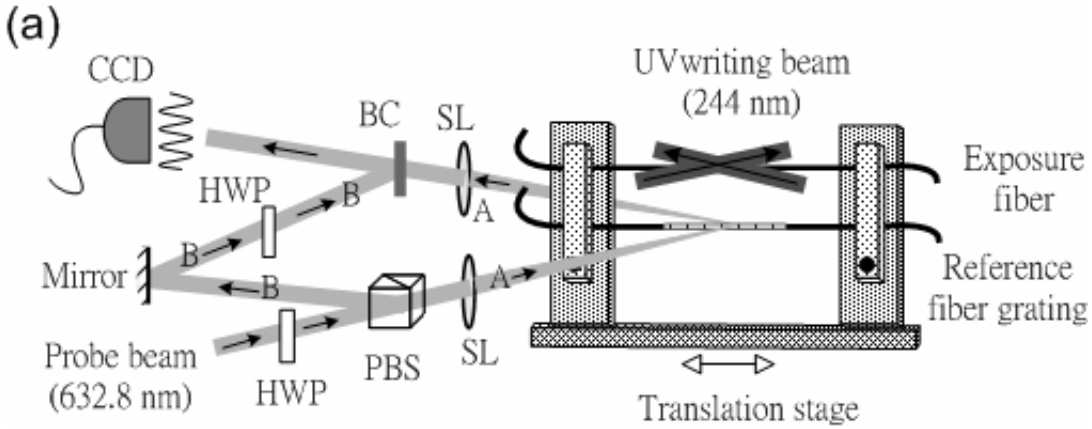


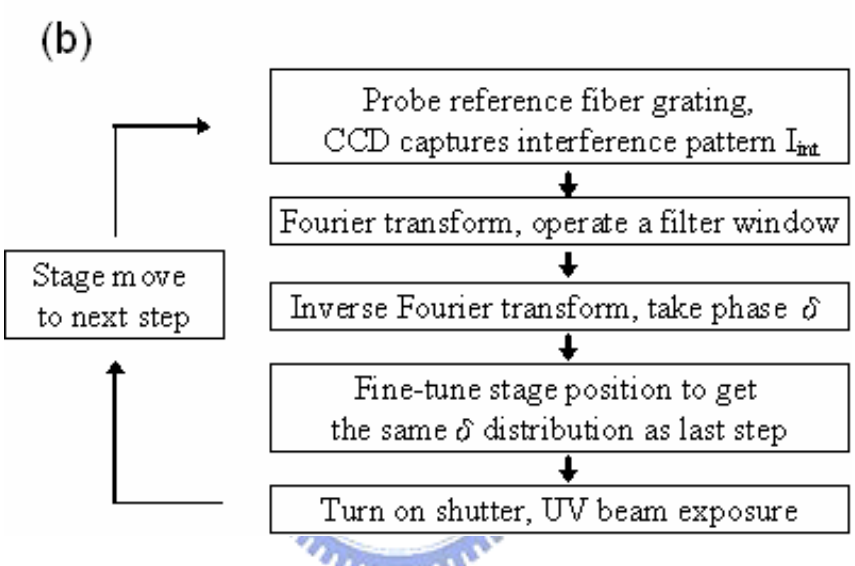


Fig. 3.5. (a) Real-time side-diffraction position monitoring setup by probing the reference grating. (b) Flow chart of the algorithm.

(a)

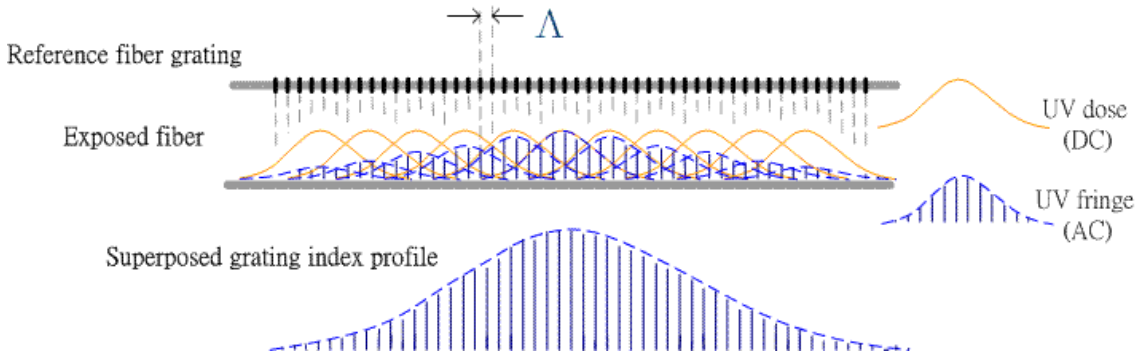


(b)

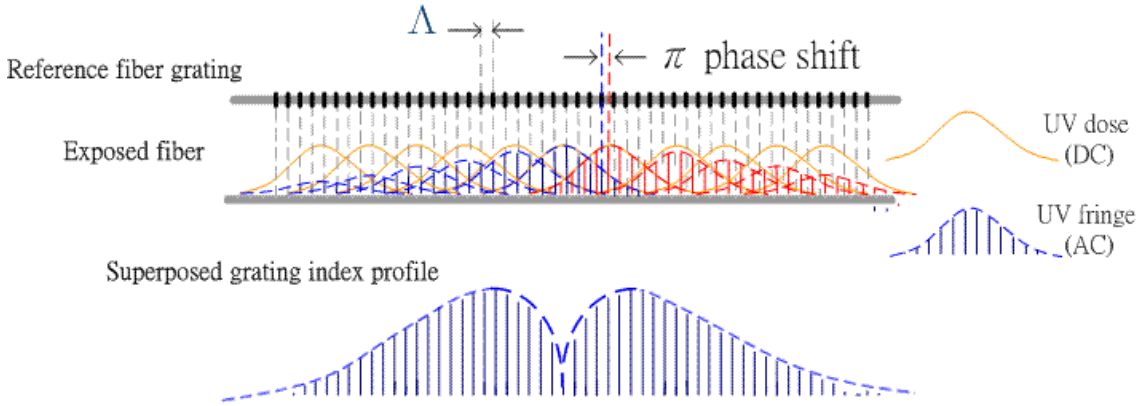


Fig. 3.6. (a) Illustration of side-diffraction interferometric position monitoring method to fabricate Gaussian apodized FBG. (b) Illustration of side-diffraction interferometric position monitoring method to fabricate phase-shifted Gaussian apodized FBG.

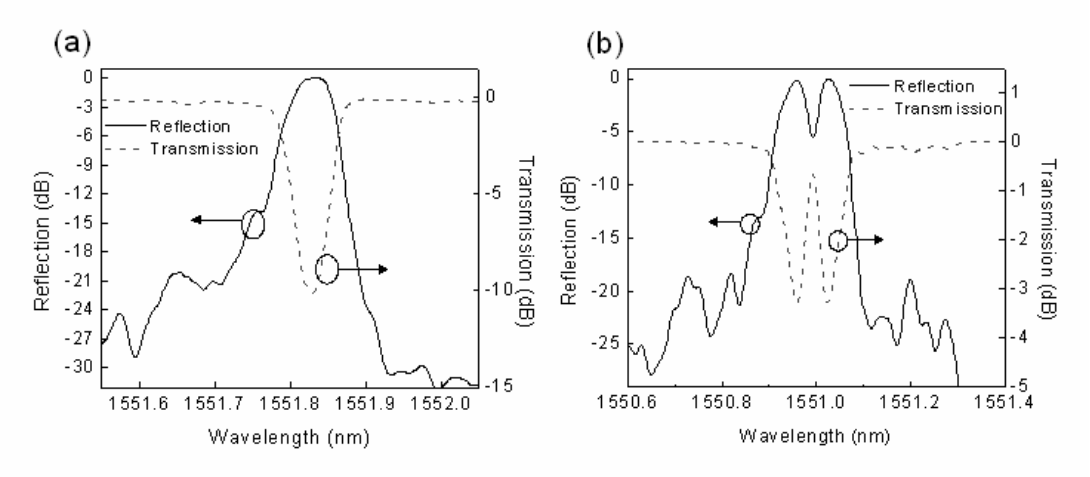


Fig. 3.7. (a) Reflection and transmission spectra of a 0.07-nm Gaussian apodized 70-mm long FBG. (b) Reflection and transmission spectra of a 40-mm long, π-phase-shift Gaussian apodized FBG.

# Chapter 4

# Methods of Achieving Linear Index-Change Response for Narrow-Band Fiber Bragg Grating Sequential Writing

## 4.1 Introduction

Fiber Bragg grating (FBG) devices as narrowband filters and dispersion compensators have numerous applications in Dense-Wavelength-Division-Multiplexing (DWDM) systems and fiber lasers [4.1,4.2]. FBGs with complex grating index profiles and multiple phase shifts can also be inversely designed to perform advanced filtering functions [4.3-4.5].The relationship between the UV flux to which the device is exposed and the induced refractive index change must be calibrated carefully in fabricating precisely these complex grating profiles and phase-shifts. The induced index change in the fiber core is not a linear function of the exposed UV flux but a complicated curve [4.6]. The curve is nonlinear at low UV flux and linear elsewhere before saturation. For narrow-band FBG devices with long grating length and small index changes, the nonlinear photosensitivity makes difficult the realization of a perfect grating profile, influencing the reflection spectrum of the grating and degrading its performance. Accordingly, the UV writing must be conducted in the linear regime, so that an FBG with an arbitrary index modulation profile can be easily realized.

Pre UV treatment is initially proposed to enhance the photosensitivity of optical fibers and increase the stability of the FBG devices [4.7], yet the advantage of the

linear index response to pre UV treatment in the matching of the target grating index profile has not been studied. In our work, the side-diffraction method is adopted to determine the refractive index profiles of fabricated FBGs more precisely. The linear grating index response is first examined using a single Gaussian UV shot with pre UV treatment. Our work demonstrates how pre UV treatment helps to achieve a linear index change with UV flux, even though two writing scans are required. An improved method of unequal two-beam interference is then proposed to generate the required AC and DC amounts of UV flux in a single writing scan. This unequal interference setup provides greater stability in writing weak gratings in the linear regime.

## 4.2 Nonlinear Photosensitivity and Pre UV Treatment

This work begins by calibrating more carefully than before the relationship between the induced change in the index of a photosensitive optical fiber and the UV flux to which it is exposed. The pre UV treatment method is then performed to achieve a linear index change response. Unlike in previous works [4.6,4.7], which assumed that the grating index profile was sinusoidal or uniform to fit the reflectivity, the side-diffraction method [4.8-4.12] is employed herein to scan the fiber grating and thus determine accurately the grating index modulation profile. An iterative procedure is then utilized to fit the reflection/transmission spectra, based on the transfer matrix method for determining the actual grating index modulation. The measured results reveal that the grating shape is deformed for simple writing schemes when the UV intensity is low. The relationship between the induced refractive index change and the exposed UV flux is nonlinear at low UV flux, such that the written grating index profile is deformed. As stated above, the pre UV treatment can be performed in advance to prevent the nonlinear photosensitivity in the writing of a weak grating. The

working principle of pre UV treatment is to eliminate the nonlinear region using a DC bias flux so that the index change depends linearly on the UV flux, and the induced index profiles are similar to the envelope of the holographic writing UV beam.

The experiments are performed on Fibercore (PS1500) photosensitive fibers, which were hydrogenated at a pressure of 1,500 psi at room temperature for seven days. The UV source is a frequency-doubled CW argon-ion laser with an output wavelength of 244 nm. A Gaussian-shaped UV fringe with its $1/e^2$ width about 6.5 mm was used to imprint holographically the fiber Bragg grating in the fiber core. The induced refractive index profile was determined using the side-diffraction method [4.12]. Furthermore, an ASE light source and an optical spectrum analyzer are employed to measure the spectral response. The normalized refractive index profile is used directly to calculate the reflection and transmission spectra using the transfer matrix method. An iterative procedure is then applied to fit the measured spectra to determine the peak index modulation of the entire FBG.

Figure 4.1(a) depicts the refractive index profiles that measured by the side-diffraction method for exposure to specified amounts of UV flux. The scan step of the translation stage is set to 100 μm. Figure 4.1(b) plots the fitted peak refractive index modulation as a function of the UV flux at the center of grating. As expected, the change in the refractive index of the photosensitive fiber is nonlinear at low UV flux and linear thereafter (No saturation is observed at the UV flux of interest). The lowest UV flux case (15 J/cm$^2$) in Fig. 4.1(a) corresponds to the rapidly changing exponential-shaped relationship in Fig. 4.1(b), which makes the grating index profile flat-topped. In previous works of mechanism studies [4.13], the photosensitization of optical fibers is modeled by a two-step process. The refractive index change is determined mainly by the concentration of Ge defect centers and defect sites for

hydrogen reaction. The model indicates that the change in the refractive index curve at low UV flux has an exponential form, which result agrees with the measurements in Fig. 4.1(b). Such nonlinear behavior causes the fiber grating index modulation profile to differ from the writing UV periodic intensity envelope. The shapes deform mostly at the tail edges of the Gaussian laser beam, where the UV intensity is low.

The pre UV treatment is conduced before the grating is made by pre-exposing the fiber uniformly to the UV radiation to prevent deformation of the grating index profile. Uniform UV pre-exposure is achieved by translating the stage step by step so that the 244 nm Gaussian-shaped UV beam partially overlaps to write on a large length of the photosensitive fiber, forming a uniform DC index change in advance. The pre UV flux is estimated to be around 59.5 J/cm$^2$. The pre UV flux is applied at the point between the linear region and nonlinear region in Fig 4.2(b).The middle of the pre-exposed region is then exposed to holographic Gaussian UV beam to write the FBG. Figure 4.2(a) displays the refractive index modulation profiles for specific exposed UV flux following pre UV treatment. Figure 4.2(b) plots the peak refractive index modulation as a function of the UV exposure flux at the center of the grating following pre UV treatment. Notably, the index modulation now depends linearly on the UV exposure flux and the induced grating index modulation profiles seem to be Gaussian-like. The $1/e^2$–intensity half widths of the one-shot UV used to generate grating index profile in Fig. 4.2(a) were about 6.55 mm, 6.35 mm, and 6.75 mm, similar to the UV beam width of 6.5 mm at a radius of $1/e^2$. This result establishes the linear refractive index response to UV flux after pre UV treatment. The pre UV treatment causes the operating point to jump away from the initial nonlinear regime such that the following grating writing process is entirely in the linear regime. The slopes in the linear region of Fig. 4.1(b) and in Fig. 4.2(b) are $4.15\times10^{-7}$ and $8.22\times10^{-7}$, respectively, indicating

that pre UV treatment enhanced the photosensitivity. This result is consistent with the results of previous studies which have demonstrated that photo-hypersensitivity increases the photosensitivity of optical fibers [4.7]. The pre UV treatment method is established herein to be a practical method of writing a weak fiber Bragg grating with the target index profile. The narrow-band FBGs were fabricated by using the strongly overlapping step-scan exposure scheme and the real-time interferometric side-diffraction position monitoring method [4.14] following pre UV treatment. The side-diffraction interferometric method is developed to connect the sections of gratings precisely. Our experience is that obtaining a low noise suppression ratio in the reflection spectrum of under 10 dB without pre-UV treatment is difficult because the nonlinear UV shots overlap process generates imperfections in the apodization index profile.

## 4.3 Unequal Two Beam Interference Setup for Achieving Linear Index Response

A long grating length and a weak apodized refractive index change with low noise are required to fabricate FBGs with narrow bandwidth and high side-lobe suppression ratio. In the preceding section, pre UV treatment yields a bias DC UV flux for the photosensitive optical fiber, which is demonstrated to be helpful in ensuring the linear response of the refractive index with AC UV flux. Unfortunately, the two required writing scans are time-consuming and sometimes may generate unwanted uncertainties. This work propose an improved method of interference which uses two unequal beam intensities to provide a bias DC UV flux and to apodize the grating profile at the same time during a single writing scan. Figure 4.3(a) schematically depicts the experimental setup. These two beams, A and B, have different UV fluxes of 24 J/cm$^2$ and 52.5 J/cm$^2$,

respectively. A half wave plate is placed in one arm of the two linearly polarized beam paths to achieve pure apodization in the sequential UV writing process and thus maintain the same refractive index change along the grating. The whole grating is AC-apodized by setting the two beams with the same polarization at the grating center, and slowly changing the relative polarization of the two beams until these two arms are orthogonally polarized at the grating edge, as in the previous pure apodization setup in which the intensities in the two arms were equal. [4.15] Figure 4.3(b) plots the variation of the UV flux upon unequal-intensity interference along the fiber axis of the exposed photosensitive optical fiber. When the total UV flux is kept constant along the whole grating, the mean change in the DC index is constant along the grating, achieving true apodization. However, the improved setup turns about 7.5 % of the maximum AC UV flux into constant DC bias flux under the same UV exposure conditions, as compared to the true apodization setup in which the intensities of the two arms are equal. Accordingly, the rapidly changing nonlinear index response regime can be avoided from the beginning and the gratings can be inscribed linearly. An experiment is carried out by fabricating a narrow-bandwidth Gaussian apodized FBG with a large length to confirm the feasibility of this proposal. The FBG is connected section by section by several 1.2 mm-spaced UV shots to a total length of 6 cm. Figure 4.4(a) compares the scanned index profile with the target profile. The tail edges are smooth and match the target Gaussian envelope, suggesting the effectiveness of the scheme. Figure 4.4(b) shows the reflection and transmission spectra of the fabricated FBG. The side-lobes are suppressed below 20 dB and the 3 dB bandwidth is approximately 0.05 nm. The peak refractive index change is $3.3\times10^{-5}$, as determined by simulation fitting. Compared with the equal-intensity interference setup for a given total UV flux, this improved setup is effective in writing FBGs to match the designed

index profile. The two beam intensity ratio can be further adjusted to optimize the performance.

## 4.4 Summary

In conclusion, the nonlinear relationship between the exposed UV flux and the induced index change of the FBGs has been calibrated more carefully than before using the side-diffraction method to determine the grating profile. The pre UV treatment method was demonstrated to eliminate the nonlinear index change response regime when the UV flux is low. An alternative new method of unequal two-beam interference was demonstrated to be able to ensure further that the shape of the induced index profile matched the targeted apodized envelope. We assert that the methods and the results presented here should be very useful in fabricating long narrow-band FBGs with weak refractive index profiles.

## 4.5 References


[4.1] Xiaoxu Li, Cheolhwan Kim, and Guifang Li, "All-optical passive clock extraction of 40 Gbit/s NRZ data using narrow-band filtering," Opt. Express **12,** 3196-3203 (2004).

[4.2] T. Qiu, S. Suzuki, A. Schülzgen, L. Li, A. Polynkin, V. Temyanko, J. V. Moloney, and N. Peyghambarian, "Generation of watt-level single-longitudinal-mode output from cladding-pumped short fiber lasers," Opt. Lett. **30,** 2748-2750 (2005).

[4.3] L.-G. Sheu, K.-P. Chuang, and Y. Lai, "Fiber Bragg grating dispersion compensator by single-period overlap-step-scan exposure", IEEE Photon. Tech.

Lett. **15,** 1557-1559 (2003).

[4.4] K. Kolossovski, R. Sammut, A. Buryak, and D. Stepanov, "Three-step design optimization for multi-channel fibre Bragg gratings," Opt. Express **11**, 1029-1038 (2003).

[4.5] C.-L. Lee, R.-K. Lee, and Y.-M. Kao, Opt. Express 14, (2006) 11002-11011.

[4.6] H. Patrick, and S. L. Gilbert, "Growth of Bragg gratings produced by continuous-wave ultraviolet light in optical fiber," Opt. Lett. **18,** 1484-1486 (1993).

[4.7] A Canagasabey, J. Canning ,and N. Groothoff, "355-nm hypersensitization of optical fibers," Opt. Lett. **28,** 1108-1110 (2003).

[4.8] P. A. Krug, R. Stolte, R. Ulrich, "Measurement of index modulation along an optical fiber Bragg grating," Opt. Lett. **20,** 1767-1769 (1995).

[4.9] J. Canning, M. Janos, M. G. Sceats, "Rayleigh z-Scan profiling of grating structures and resonances in optical fibres using side-scattered light," 20th Australian Conference on Optical Fibre Technology (ACOFT-20), Coolum, Queensland, 303-306, (December, 1995);

[4.10] J. Canning, M. Janos, M.G. Sceats, "Rayleigh longitudinal profiling of optical resonances within waveguide grating structures using sidescattered light," Opt. Lett. **21,** 609-611 (1996).

[4.11] Baskin LM, Sumetsky M, Westbrook PS, Reyes PI, Eggleton BJ, "Accurate characterization of fiber Bragg grating index modulation by side-diffraction technique," IEEE Photon. Technol. Lett. **15,** 449-451 (2003).

[4.12] F. El-Diasty, A. Heaney, and T. Erdogan, "Analysis of fiber Bragg gratings by a side-diffraction interference technique," Appl. Opt. **40,** 890-896 (2001).

[4.13] John Canning, "Photosensitization and photostabilization of laser-induced

index changes in optical fibers," Opt. Fiber Tech. **6,** 275-289 (2000).

[4.14] K.-C. Hsu, L.-G. Sheu, K.-P. Chuang, S.-H. Chang, and Y. Lai, "Fiber Bragg grating sequential UV-writing method with real-time interferometric side-diffraction position monitoring," Opt. Express **13,** 3795-3801 (2005).

[4.15] K.-P. Chuang, Y. Lai, and L.-G. Sheu, "Pure apodized phase-shifted fiber Bragg gratings fabricated by a two-beam interferometer with polarization control," IEEE Photon. Technol. Lett. **16,** 834-836 (2004).

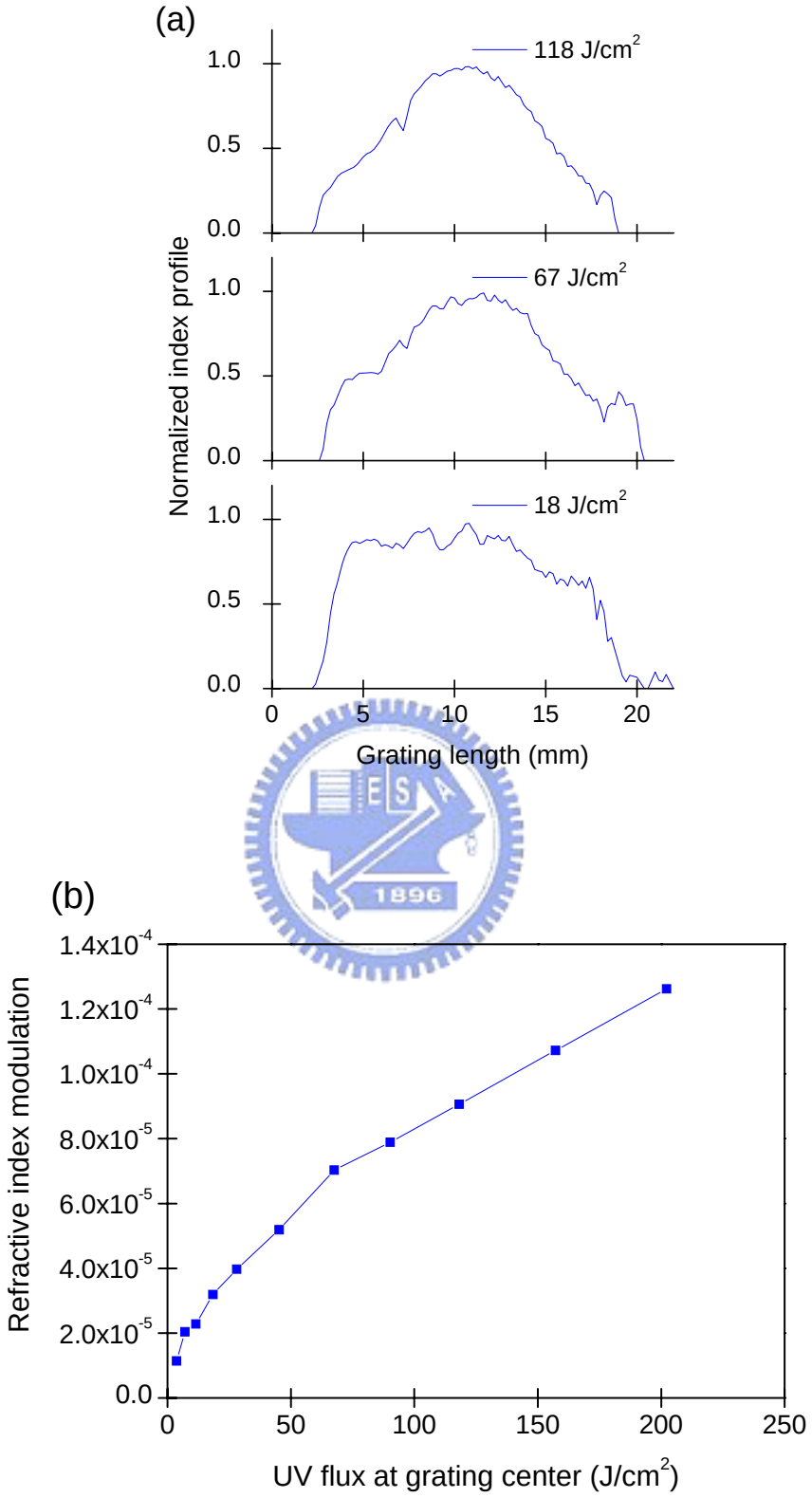


Figure 4.1. (a) Refractive index modulation profile of a single Gaussian shot UV writing with specific UV flux. (b) Refractive index modulation versus UV exposure flux.

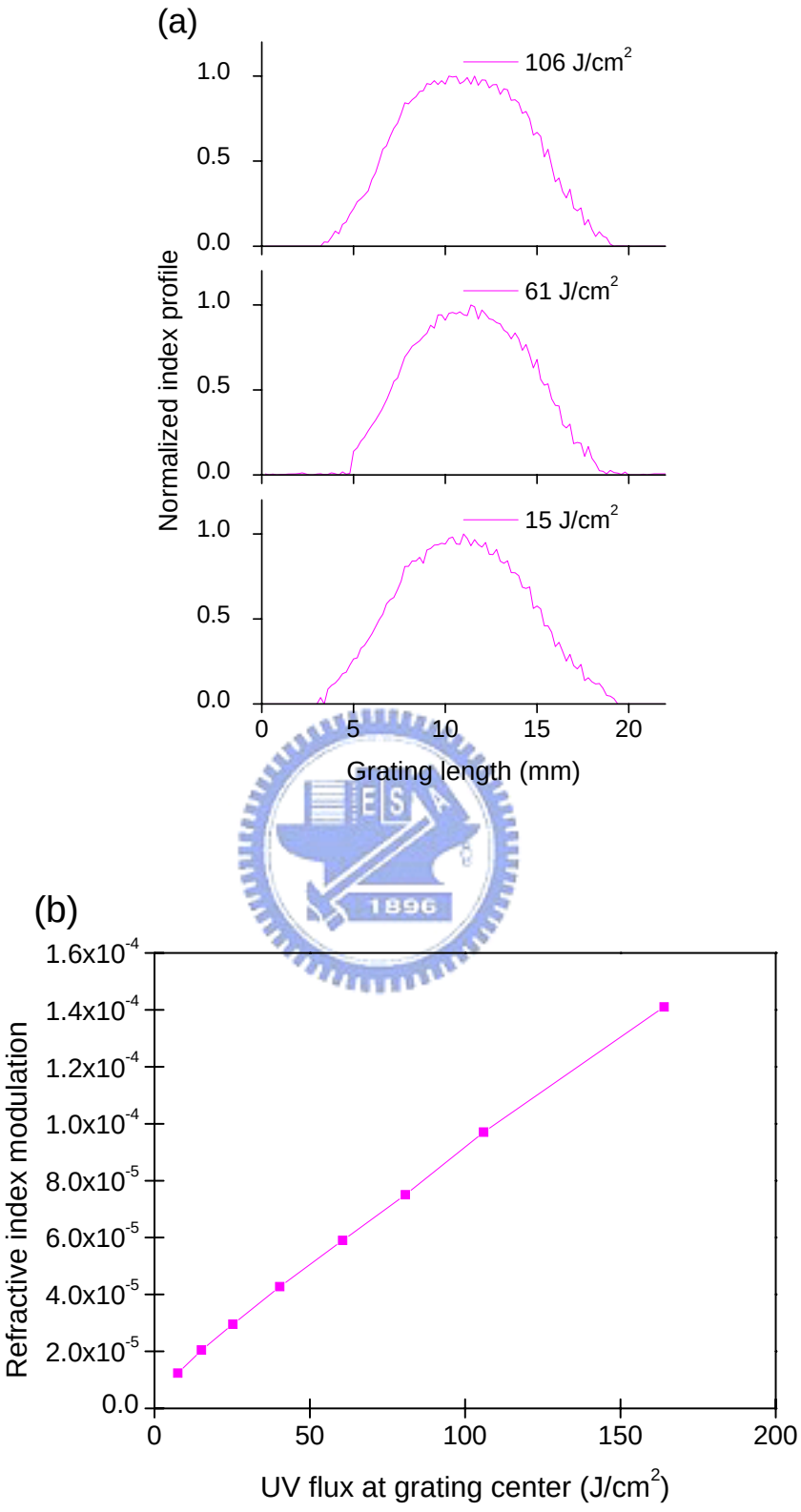


Figure 4.2. (a) Refractive index modulation profiles with pre UV treatment of a single Gaussian shot UV writing with specific UV flux. (b) Refractive index modulation versus UV exposure flux with pre UV treatment.

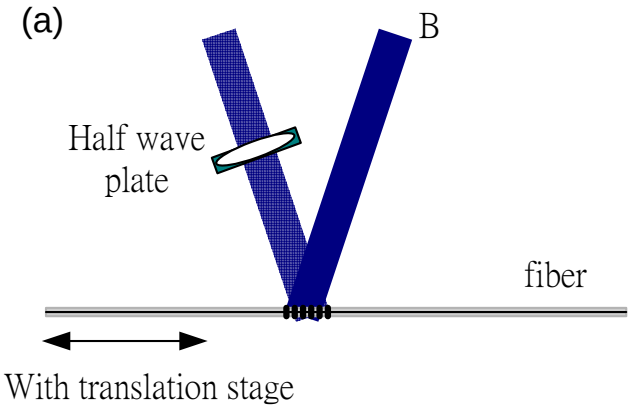


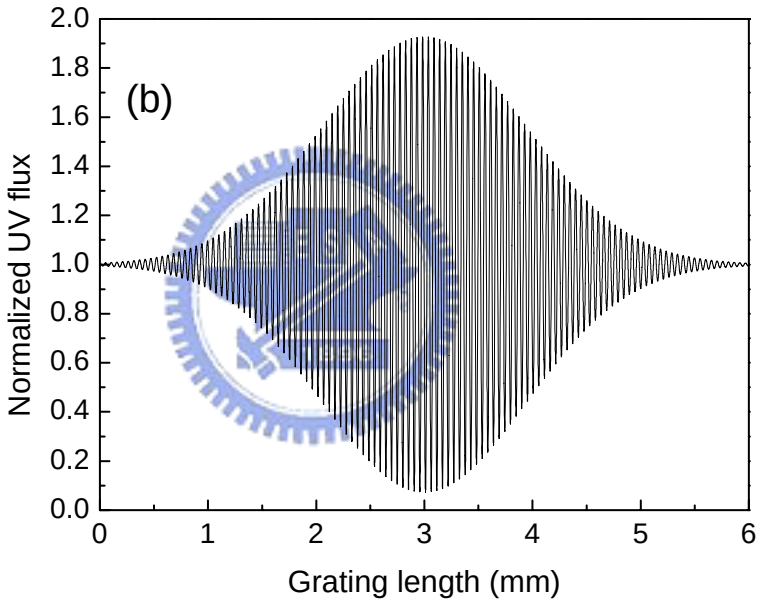


Figure 4.3. (a) Experimental setup of unequal-intensity two beam interference. The intensity ratio of beam A and beam B is 0.45. (b). Illustration of UV flux variation versus grating length with unequal-intensity two beam interference setup.

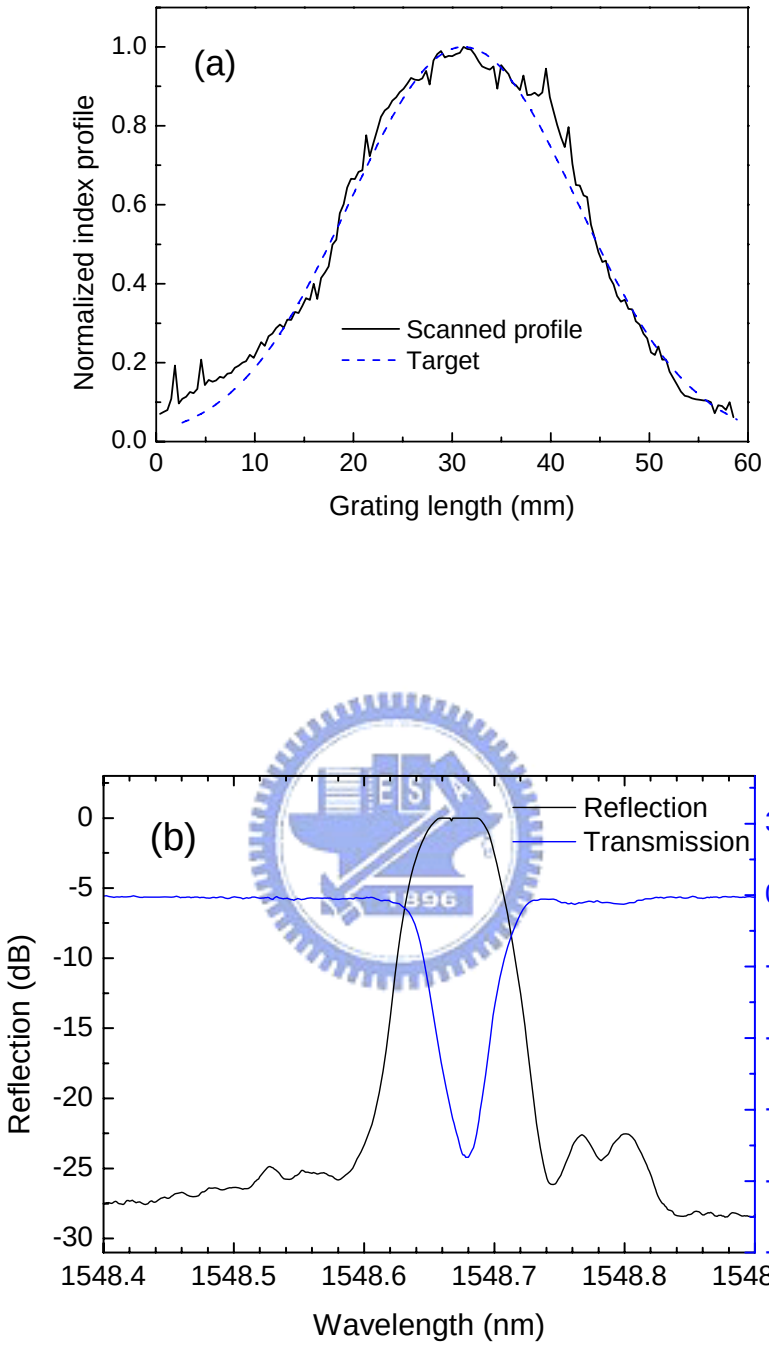


Figure 4.4. (a) Refractive index modulation profiles for experimental and target gratings with unequal-intensity two beam UV writing. (b) Reflection and transmission spectrum of the grating with unequal-intensity two beam UV writing.

# Chapter 5

# Simple Pure Apodization Method for Fiber Bragg Gratings by Sequential UV Writing

## 5.1 Introduction

Many pure apodization methods for realizing advanced fiber Bragg gratings (FBGs) have been developed during the past few years to achieve high quality filtering functions [5.1-5.8]. FBGs as narrowband filters have important applications in single-longitudinal mode fiber lasers and DWDM systems [5.9,5.10]. The required narrow-band is achieved by long grating length, while the high sidelobe suppression ratio is achieved by pure apodization. Here pure apodization means to keep the average refractive index to be constant through the entire grating length while the ac index modulation can change independently. Previous developed technologies include the double-ultraviolet exposure method, complex design of phase mask, moving-fiber scanning-beam dithering technique, phase mask method with polarization control, and two beam interference with polarization control. However, these methods may suffer from the introduction of additional uncertainties, requiring additional optical elements, limitation of grating length, or only being suitable in either phase mask or holographic approach. In this work, a simple and cost-effective FBG writing method is proposed to realize pure apodization for both the phase mask and holographic sequential UV writing schemes. The UV dose exposed on the fiber to form every grating section is divided into two sequentially writing shots instead of one. In this way one gain the freedom to adjust the ac-index independently while keeping the dc index profile fixed through the whole grating length. Meanwhile, the grating phase kept continued at

every exposure location to precisely connect grating sections with partial overlap to form the desire grating profile. Narrow-band FBGs are experimentally demonstrated, and tolerance analysis is given using the proposed method.

## 5.2 Theory and Experiment

For long FBG fabrication by the sequential UV writing scheme, Gaussian-shaped writing beam is equally-spaced and partially-overlapped to sequentially imprint grating sections. The phases of the overlapped grating sections must be controlled precisely to form a long-length grating without phase errors. The average refractive index ($n_{dc}$) has to be constant along the fiber while the ac index modulation ($n_{ac}$) can be locally changed to form specific apodized profiles. The schematic diagram of writing a cos-squared apodized FBG by sequential UV writing process is shown in Fig. 5.1(a). The exposure locations are equal-spaced and are denoted as $x_i$, i = 1, 2….N, and let the UV dose to be $2I_0$ at every equal-spaced $x_i$. For a cos-squared apodized FBG, the UV fringe is maximum at the grating center, and minimum at the grating tail, and the total UV dose at $x_i$ is the same.

To achieve pure apodization, two exposure configurations are proposed. The total UV dose, $2I_0$, is divided into two shots, shot 1 and shot 2, with the beam amplitudes $I_1$ and $I_2$, respectively, and the phases of the two sequentially writing UV fringes are $\theta_1$ and $\theta_2$, respectively. The index modulation amplitude and phase of every grating section are determined by the superposition of the two shot profiles, as shown in Eq. 5.1.

$$I(x) = I_1 e^{i(kx+\theta_1)} + I_2 e^{i(kx+\theta_2)} \propto \quad n_{dc}(x) + n_{ac}(x) \,. \tag{5.1}$$

In configuration 1, the total UV dose is $2I_0$, and the two sequentially writing shots have equal amplitude $I_0$. The ac index modulation is adjusted by symmetrically

changing the fringe phase of the two shots to be $\Delta\theta$ and $-\Delta\theta$, as shown in Fig. 5.1(b). Expected zero phase-shift at $x_i$ after superposing is achieved by the symmetrically phase shifts of two sequentially writing shots. Equation 5.2 shows the superposed UV fringe distribution, which amplitude can be determined by the factor $\cos(\Delta\theta)$. Table 5.1 shows some example conditions of the two sequentially writing shots in this configuration.

In configuration 2, the index modulation is achieved by setting $\theta_1$ and $\theta_2$ equal to 0 and $\pi$, respectively, and let the amplitude $I_1 = mI_0$. The total UV dose is $2I_0$. Equation 5.3 shows the superposed UV fringe amplitude distribution. Expected zero phase-shift at $x_i$ after superposing is achieved by the fixed $\pi$ phase shifts of two sequentially writing shots. The final fringe amplitude is determined by the factor (m-1). Table 5.1 shows some example conditions of the two shots in this configuration.

$$I(x) = 2I_0 e^{ikx} \cos(\Delta\theta) , \tag{5.2}$$

$$I(x) = 2I_0 e^{ikx} (m-1) . \tag{5.3}$$

The proposed methods have been experimentally tested by exposing photosensitive optical fibers to 244-nm UV radiation, which has the Gaussian-shaped UV fringe with its $1/e^2$ width about 6.5 mm. The UV dose for achieving maximum index modulation is divided into two shots, and sequentially exposes onto the fiber at the same location. To ensure linear index response, the fibers are performed with UV treatment in advance [5.11]. The grating index modulation envelopes are measured by side-diffraction method [5.11] and the transmission dips are measured by the optical spectrum analyzer. Figures 5.2(a) and 5.2(b) show some measured grating index profiles. The index modulation profiles of the gratings are Gaussian-shaped, similar to the shape of UV writing profile. By using the measured Gaussian index envelopes in the transform matrix calculation to fit the transmission spectra, the curve between the

normalized index modulation and phase shift $\Delta\theta$ is shown in Fig. 5.2(c), and the curve between the normalized index modulation and $m=I_1/I_0$ is shown in Fig. 5.2(d). The simulation curves in Figs 5.2(c) and 5.2(d) are derived from Eq. 5.2 and Eq. 5.3. The experimental data in dots fit well with the theoretical predictions in Eq. 5.2 and Eq.5.3.

The feasibility of the proposed method is verified by connecting grating sections to form a cos-squared apodized FBGs with a constant DC refractive index modulation along the whole grating. The real-time interferometric side-diffraction method [5.11] is utilized for sequential UV writing. The Gaussian-shaped UV fringe has its $1/e^2$ width about 6.5 mm and the fiber scan step is about 1.6 mm. The final FBG is produced after a 35-section sequential writing to reach a total grating length about 50 mm. Before the UV writing process, a DC pre-UV treating process is applied to avoid the nonlinear regime when the exposure UV flux is small. Figures 5.3(a) and 5.3(b) show the envelope of index modulation profile for the produced FBG utilized configuration 1 and configuration 2, respectively, and Figs. 5.3(c) and 5.3(d) show the reflection and transmission spectra of the exposed FBG connected by grating sections utilizing configuration 1 and configuration 2, respectively. The reflection spectrum has a relatively flat top with the sidelobe level below -20 dB in both configurations. The 3-dB bandwidth of the reflection spectrum is only 0.088 nm and 0.083 nm in configuration 1 and configuration 2, respectively. The peak refractive index modulation is $3.76\times10^{-5}$ for this 50-mm long cos-squared apodized FBG, determined by simulation-fitting. This example demonstrates the feasibility for fabricating long fiber Bragg gratings without noticeable phase errors. This proposed method needs no additional elements and easy to integrate into real-time interferometric side-diffraction method, while the take-time is slightly increased on finding the fiber phase than our previous setup.

The fabrication tolerance is evaluated by random position error for FBG sequential writing. Simulation of random phase errors caused by random position errors is added to every grating section to show how they affect transmission rate and side lobe suppression ratio. The three cases of interest are that the UV dose exposed on the fiber to form every grating section to be one shot (case 1), and to be two sequentially writing shots as proposed configuration 1 (case 2) and configuration 2 (case 3). Table 5.2 shows the average and variance result on spectral characteristic of transmission dip and sidelobe suppression ratio in three cases under the error condition of 0%, 1%, 5% and 10% of grating period. In all cases, the position error slightly effects transmission dip of connected FBGs, but greatly affects the performance of sidelobe suppression ratio. When position error is smaller than 5% of grating period, the degrade rate of side lobe suppression ratio for both configurations are at the same level in with case 1. This verifies that two configurations have good resistance to random phase error in practical production.

## 5.3 Summary

In conclusion, a simple method for attaining pure apodization is proposed for FBG sequential UV writing. The UV dose at every exposed location is divided into two, and the ac index modulation is adjusted by controlling the superimposed phase and amplitude of the two sequentially imprinted UV fringes. The average refractive index is kept constant due to the constant net UV flux per grating section, and the ac index modulation can be locally and independently changed in both configurations. Experimental results and tolerance analysis are given to show the feasibility of both configurations in connecting grating sections.

# 5.4 References


[5.1] W. H. Loh, M. J. Cole, M. N. Zervas, S. Barcelos, and R. I. Laming, "Complex grating structures with uniform phase masks based on the moving fiber–scanning beam technique," Opt. Lett. **20,** 2051-2053 (1995).

[5.2] K.-P. Chuang, L.-G. Sheu, and Y. Lai, "Pure apodized phase-shifted fiber Bragg gratings fabricated by a two-beam interferometer with polarization control", IEEE Photon. Technol. Lett. **16,** 834-836 (2004).

[5.3] Kai-Ping Chuang and Yinchieh Lai, and Lih-Gen Sheu, "Complex fiber grating structures fabricated by sequential writing with polarization control," Opt. Lett. **29,** 340–342 (2004).

[5.4] Y. Nasu and S. Yamashita, "Densification of sampled fiber Bragg gratings using multiple-phase-shift (MPS) technique," J. Lightwave Technol. **23,** 1808-1817 (2005).

[5.5] B. Malo, S. Theriault, D. C. Johnson, F. Bilodeau, J. Albert, and K. O. Hill, "Apodised in-fiber Bragg grating reflectors photoimprinted using a phase mask," Electron. Lett. **31,** 223–225 (1995).

[5.6] J. Albert, K. O. Hill, B. Malo, S. Theriault, F. Bilodeau, D. C. Johnson, and L. E. Erickson, "Apodisation of the spectral response of fiber Bragg gratings using a phase mask with variable diffraction efficiency," Electron. Lett. **31,** 222-223 (1995).

[5.7] C. Yang and Y. Lai, "Apodised fiber Bragg gratings fabricated with uniform phase mask using low cost apparatus," Electron. Lett. **36,** 655-656 (1995).

[5.8] Jesper Bo Jensen, Nikolai Plougmann, Hans-Jürgen Deyerl, Poul Varming, Jörg Hübner, and Martin Kristensen, "Polarization control method for ultraviolet writing of advanced Bragg gratings," Opt. Lett. **27,** 1004-1006 (2002).

[5.9] E. Wikszak, J. Thomas, J. Burghoff, B. Ortaç, J. Limpert, S. Nolte, U. Fuchs, A. Tünnermann, “Erbium fiber laser based on intracorefemtosecond-written fiber Bragg grating” Opt. Lett., **31,** 2390–2392 (2006).

[5.10] A. Schülzgen, L. Li, V. L. Temyanko, S. Suzuki, J. V. Moloney, and N. Peyghambarian, “Single-frequency fiber oscillator with watt-level output power using photonic crystal phosphate glass fiber,” Opt. Express **14,** 7087-7092 (2006).

[5.11] Kuei-Chu Hsu, Lih-Gen Sheu, Kai-Ping Chuang, Shu-Hui Chang and Yinchieh Lai, “Fiber Bragg grating sequential UV-writing method with real-time interferometric side-diffraction position monitoring,” Opt. Express **13,** 3795-3801 (2005).

(a)

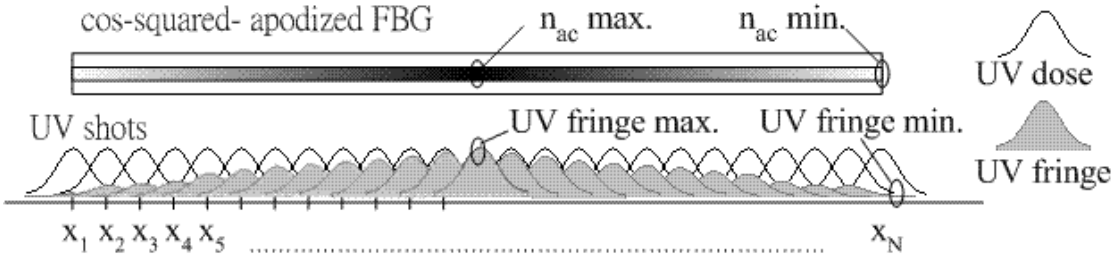


(b)

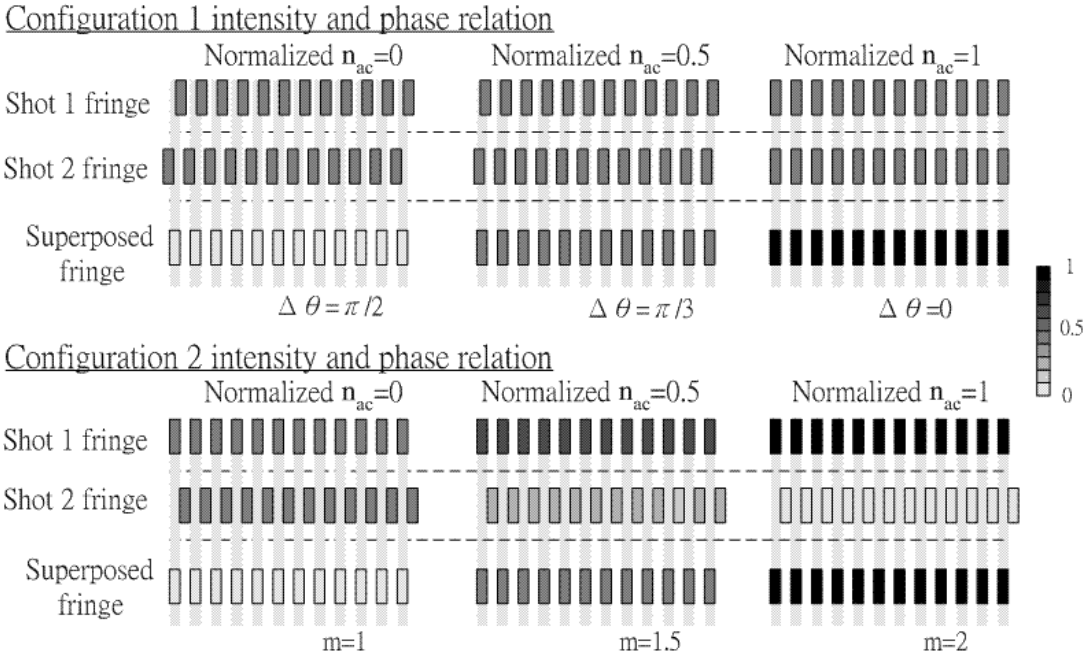


(b)

Figure 5.1. (a) Schematic of UV sequential writing. (b) Superposed UV fringe by controlling intensities and phases of the two sequentially writing shots.

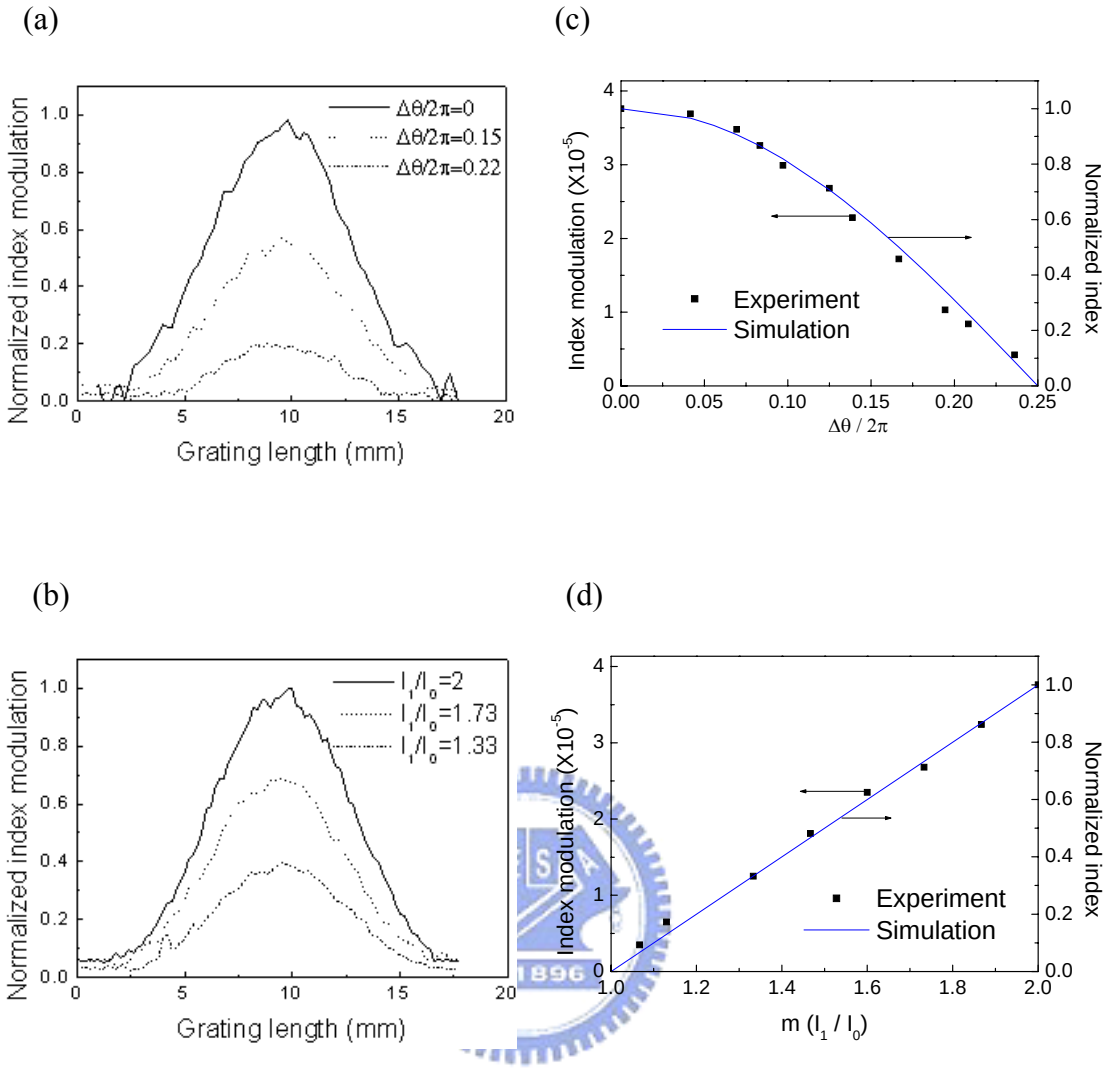


Figure 5.2. Index profiles of single grating section utilized (a) configuration 1 and (b) configuration 2. Experimental and simulation of index modulation of single grating section utilized (c) configuration 1 and (d) configuration 2.

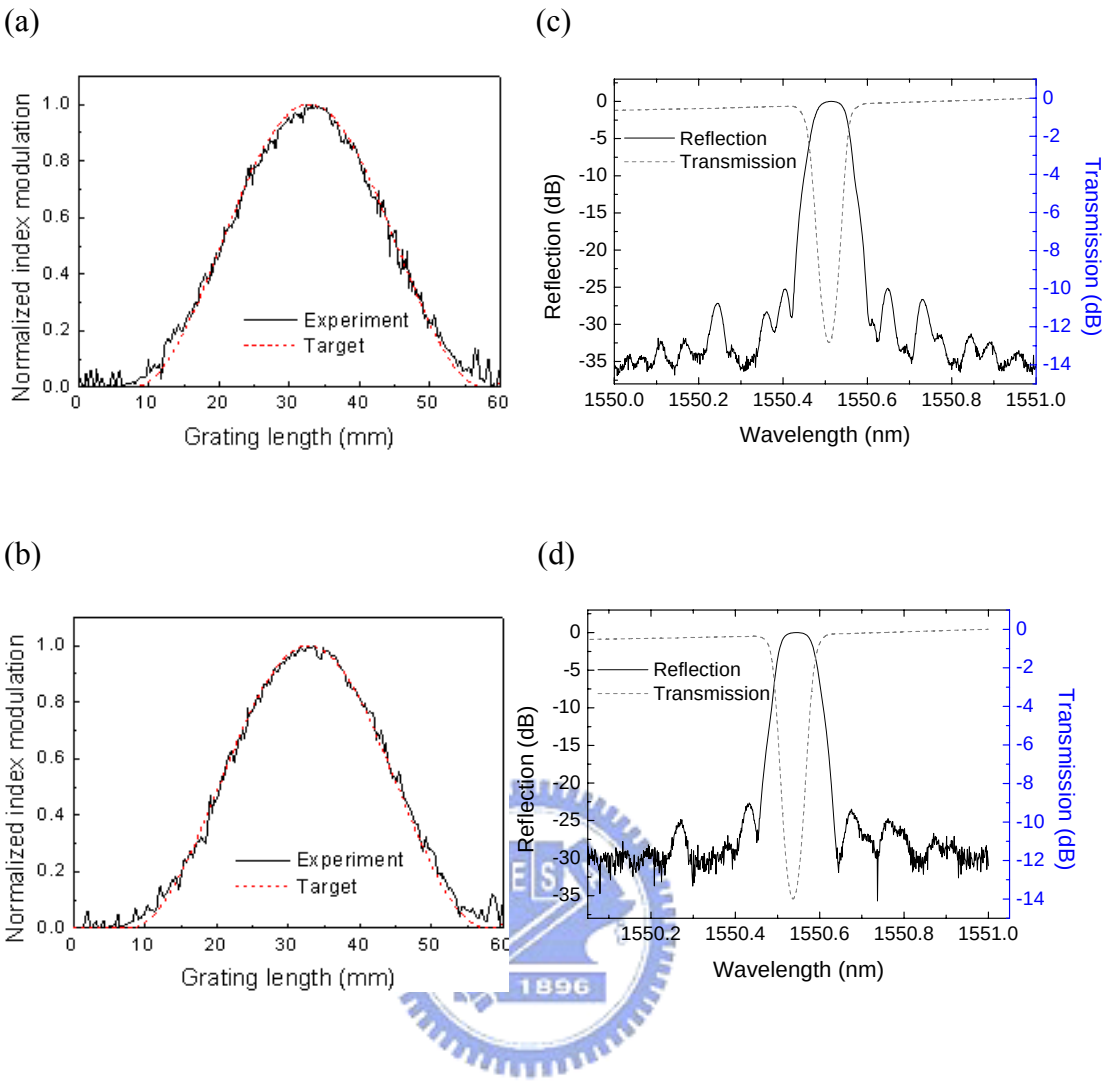


Figure 5.3. Connected FBG index profile utilized (a) configuration 1 and (b) configuration 2. Connected FBG reflection and transmission spectrum utilized (c) configuration 1and (d) configuration 2.

| | Configuration 1<br>$\theta_1 = -\theta_2 = \Delta\theta$<br>$I_1 = I_2 = I_0$ | Configuration 2<br>$\theta_1 = 0, \theta_2 = \pi$<br>$I_1 = mI_0, I_1 + I_2 = 2I_0$ |
|---|---|---|
| Normalized<br>$n_{ac} = 1$ | $\Delta\theta = 0$ | $m = 2$ |
| Normalized<br>$n_{ac} = 0.5$ | $\Delta\theta = \pi / 3$ | $m = 1.5$ |
| Normalized<br>$n_{ac} = 0$ | $\Delta\theta = \pi / 2$ | $m = 1$ |

Table 5.1 The conditions of the two configurations.

| | Transmission (dB) | | | Side lobe suppression ratio (dB) | | |
|---|---|---|---|---|---|---|
| | Case 1 | Case 2 | Case 3 | Case 1 | Case 2 | Case 3 |
| Error of period | Average/ deviation | Average/ deviation | Average/ deviation | Average/ deviation | Average/ deviation | Average/ deviation |
| 0% | 15.36 / | 15.36 / | 15.36 / | 35 / | 35 / | 35 / |
| 1% | 15.36 / 0.003 | 15.33 / 0.09 | 15.36 / 0.004 | 32.73 / 1.20 | 31.92 / 2.55 | 31.17 / 1.55 |
| 5% | 15.12 / 0.06 | 15.05 / 0.52 | 15.17 / 0.086 | 24.40 / 2.63 | 21.87 / 3.45 | 20.83 / 2.77 |
| 10% | 14.47 / 0.23 | 14.26 / 1.07 | 14.60 / 0.42 | 17.79 / 3.69 | 15.60 / 3.17 | 14.43 / 3.33 |

Table 5.2 Simulation of how random position error contributes to transmission and sidelobe suppression ratio in one shot case and two configurations.

# Chapter 6

# Conclusions and Future Work

## 6.1 Conclusions

Complex FBG structures of arbitrary phase shifts and refractive index profiles have been continuously attractive for many optical applications. To develop the state-of-the-art FBG fabrication technique, in this dissertation we have proposed and demonstrated several advanced FBG fabrication methods for achieving pure apodization, long grating length with sequential UV writing, and better linear index response.

This dissertation firstly presents a new sequential UV-writing procedure for fabricating long fiber Bragg grating (FBG) devices in Chapter 3. In the literature, several procedures that can realize long and complex FBG structures have recently been developed. However, the accumulative position reading errors have caused significant difficulties on the fabrication of long-length fiber Bragg gratings. Based on the side-diffraction method, we have proposed and demonstrated a real-time fiber position monitoring method for sequential UV-writing processes, in order to be able to write long-length gratings accurately. To real-time accurately align the position of every exposed FBG section prior to UV exposure, a single-period reference fiber grating with strong refractive index modulation is probed by applying an interferometric side-diffraction method to measure the grating phase as the position reference. In this way the overlapped FBG sections can be connected section-by-section without obvious phase errors, even when the written

index-modulation is weak.

To realize FBGs with arbitrary refractive index profiles and arbitrary phase shifts, it is necessary to calibrate the relationship between UV beam exposure duration versus refractive index change. In Chapter 4, we elucidate the refractive index change response of the photosensitive optical fiber to exposed UV flux. The nonlinear UV photosensitivity deforms the index profile of FBGs on the tail edges where the writing UV flux is low. Pre UV treatment eliminates the nonlinear index-change response and ensures the linearity of the response of subsequent grating writing. A new method that involves interference between two unequal beams in a single writing scan is proposed and demonstrated to be able to improve the index profile and the spectral response of fabricated FBGs. The procedure is stable for writing weak fiber Bragg gratings with pre-designed index profiles.

In Chpater 5, a simple UV exposure method is proposed to achieve pure apodization for fiber Bragg gratings fabricated by sequential UV writing. Through the exposure phase and/or time control of multiple UV shots, the ac-index can be adjusted independently with the dc-index kept constant. The UV dose exposed on the fiber to form every grating section is divided into two sequentially writing shots instead of one. In this way one gains the freedom to adjust the ac-index independently while keeping the dc index profile fixed. By precisely connecting grating sections with partial overlap, the desire grating profile can be matched while the dc index become constant through the whole grating length. The proposed simple and cost-effective FBG writing method is able to realize pure apodization for both the phase mask and holographic sequential UV writing schemes

Based on the developed grating inscription skills and calibration results in this dissertation, we have developed an excellent fiber grating fabrication platform which

has the potential to be able to produce complex and advanced FBGs for various applications.

## 6.2 Future Work

This dissertation demonstrates improved FBG fabrication methods which are proven to be feasible. Future work on FBG development along this line are listed in the following sections, including complex FBG fabrication, FBG sensor applications, and FBGs in fiber lasers.

### 6.2.1 Complex FBG Fabrication

Since our goal is to develop a plateform to fabricate various kinds of FBGs, the next work is to actually realize a more complicated designed grating structure. In the past years, our group have tried some numerical simulation methods to inversely design the detail parameters of FBG structures from a given spectrum [6.1,6.2]. The FBG fabrication can be carried out in principle by the proposed techniques in Chapter 3, 4, and 5. However, smaller UV writing beam size is required to be able to fit the severely changed grating index profiles. Take Ref. [6.2] for example, the multi-channel FBG structure is very difficult to realize by using the ordinary partially-overlapped sequential writing process with the Gaussian-shaped UV fringe with its $1/e^2$ width about 6.5 mm. For this case, we will use smaller UV writing beam size to fit the target index profile, and sequentially write the profile into the fiber by using the side-diffraction method for real-time monitoring and by the new pure apodization method. Furthermore, the reference fiber grating used in Chapter 3 makes the optical alignment difficult because of the small fiber radius and the weak diffraction efficiency.

The idea of replacing the reference fiber grating with a phase mask as a position reference is considered. Though the phase mask has the period twice of the written grating, the reliable accuracy of the period and the stable properties makes the phase mask a good candidate as the reference for position monitoring. The work is already going on right now.

### 6.2.2 FBG Sensor Applications

Fiber Bragg grating-based sensing has proven to be a very fertile research area, and new developments can be expected to continue over the next few years. Gratings are simple, intrinsic sensing elements which can be photo-inscribed into a silica fiber. Grating-based sensors appear to be useful for a variety of applications, including refractive index, temperature, and tension sensing. Our next work is trying to apply FBGs and LPGs into environmental sensing.

### 6.2.3 FBGs in Fiber Lasers

Many research works have been focused on the development of 1 $\mu$m mode-locked Yb-fiber lasers recently, since 1 $\mu$m femtosecond pulsed source are useful in many applications, such as multiphoton microscopy [6.3], supercontinuum generation for optical coherent tomography (OCT) [6.4], and high-repetition-rate femtosecond combs for precise frequency metrology [6.5]. Our group had achieved 1.55 $\mu$m femtosecond Er-fiber lasers, and can also apply to 1 $\mu$m femtosecond Yb-fiber lasers. FBGs written in Yb-doped photosensitive fiber to directly form a DBR fiber laser is our next project.

## 6.3 References


[6.1] L.-G. Sheu, K.-P. Chuang, and Y. Lai, “Fiber Bragg grating dispersion compensator by single-period overlap-step-scan exposure,” IEEE Photon. Technol. Lett. **15,** 939-941 (2003).

[6.2] C.-L. Lee, R.-K. Lee, and Y.-M. Kao, “Design of multichannel DWDM fiber Bragg grating filters by Lagrange multiplier constrained optimization,” Opt. Express **14,** 11002-11011 (2006).

[6.3] T.-H. Tsai, S.-P. Tai, W.-J. Lee, H.-Y. Huang, Y.-H. Liao, and C.-K. Sun, “Optical signal degradation study in fixed human skin using confocal microscopy andhigher-harmonic optical microscopy,” Opt. Express **14**, 749 (2006).

[6.4] H. Lim, Y. Jiang, Y. Wang, Y.-C. Huang, Z. Chen, and F. W. Wise,“Ultrahigh-resolution optical coherence tomography with a fiber laser source at 1μm,” Opt. Lett. **30**, 1171 (2003).

[6.5] T. Udem, R. Holzwarth, and T. W. Hänsch, “Optical frequency metrology,” Nature **416**, 233 (2002).

# VITA

# 簡 歷

**姓 名:**

徐桂珠 (Kuei-Chu Hsu)

**學 歷:**

| | | | |
|---|---|---|---|
| 2002.9 - 2007.6 | 交通大學 | 光電工程研究所 | 博士 |
| 1998.9 - 2000.6 | 成功大學 | 物理研究所 | 碩士 |
| 1993.9 - 1997.6 | 臺灣師範大學 | 物理系 | 學士 |

**經 歷:**

| | | |
|---|---|---|
| 訪問學者 | College of Optical Sciences, the University of Arizona, USA | 2006 May~2007 Jan |
| 交換學生 | Institute of Applied Physics, Friedrich-Schiller-University Jena, Germany | 2005 July~2005 Sep |
| 產品開發工程師 | 友達光電 | 2000 Jun~2002 Oct |
| 理化專任教師 | 台北市立萬芳國中 | 1997 Aug~1998 July |

**榮 譽:**

| | |
|---|---|
| 補助博士生赴國外研究（千里馬專案） (2006) | 國科會 |
| 碩士論文獎 佳作 (2001) | 中華民國物理學會 |

# Publication List

## International journals

1. **Kuei-Chu Hsu**, Lih-Gen Sheu, Wei-Wei-Hsiang, and Yinchieh Lai, "Methods of achieving linear index-change response for narrow-band fiber Bragg grating sequential writing," accepted by Opt. Commun. (2007). (SCI)

2. Nan-Kuang Chen, **Kuei-Chu Hsu,** Sien Chi, Yin-Chieh Lai, "Tunable Er3+-doped fiber amplifiers covering S- and C + L-bands over 1490 ~ 1610nm based on discrete fundamental-mode cutoff filters," Opt. Lett. 31, 2842-2844 (2006). (SCI)

3. N. K. Chen, L. Zhang, **K. C. Hsu,** L. Hu, S. Chi, Y. Lai, S. M. Tseng, and J. T. Shy, "CW-pumped evanescent amplification based on side-polished fiber with heavily $Er^{3+}$-doped glass overlay," Jpn. J. Appl. Phys. 45, 6328-6330 (2006). (SCI)

4. Chien-Hung Yeh, Ming-Ching Lin, Ting-Tsan Huang, **Kuei-Chu Hsu**, Cheng-Hao Ko, and Sien Chi, "S-band gain-clamped grating-based erbium doped fiber amplifier by forward optical feedback technique," Opt. Express 14, 2611-2617 (2006). (SCI)

5. **Kuei-Chu Hsu**, Lih-Gen Sheu, Kai-Ping Chuang, Shu-Hui Chang and Yinchieh Lai, "Fiber Bragg grating sequential UV-writing method with real-time interferometric side-diffraction position monitoring," Opt. Express 13, 3795-3801 (2005). (SCI)

6. Wei-Ren Peng, Peng-Chun Peng, Wen-Piao Lin, **Kuei-Chu Hsu**, Yinchieh Lai, and Sien Chi, "A cost-effective fast frequency-hopped code-division multiple-access light source using self-seeded Fabry-Perot laser with fiber Bragg grating array," IEEE Photon. Technol. Lett. 16, 2550-2552 (2004). (SCI)

7. Andy Y.-G. Fuh, C.-C. Liao, **K.-C. Hsu** and C.-L. Lu, "Laser-induced reorientation effect and ripple structure in dye-doped liquid-crystal films," Opt. Lett. 28, 1179-1181 (2003). (SCI)

8. Andy Y.-G. Fuh, C.-C. Liao, **K.-C. Hsu**, C.-L. Lu and T.-S. Mo, "Laser-induced ripple structure of dopant on the substrates in a dye-doped liquid crystal cell and its alignment effect," Journal of Nonlinear Optical Physics & Materials, 11, 57-63 (2002). (SCI)

9. Andy Y.-G. Fuh, C.-C. Liao, **K.-C. Hsu**, C.-L. Lu, and C.-Y. Tsai, "Dynamic studies of holographic gratings in dye-doped liquid-crystal films," Opt. Lett. 26, 1767-1769 (2001). (SCI)

## Conferences

1. **Kuei-Chu Hsu**, and Yinchieh Lai, "Simple pure apodization method for fiber Bragg gratings by sequential UV writing," OECC 2007 conference, paper 282, Yokohama, Japan, Jul 9-13, 2007.
2. N. K. Chen, **K. C. Hsu,** S. Chi, and Y. Lai, "Tunable Er3+-doped fiber amplifiers covering S- and C+L bands (1490 ~ 1610 nm) using discrete all-fiber ASE suppressing filters," IEEE/LEOS 2006 conference, Montreal, Canada, paper TuAA5, Oct. 29 - Nov. 2, 2006.
3. N. K. Chen, **K. C. Hsu,** K. F. Hong, S. Chi, and Y. Lai, "High-cutoff-efficiency tunable short-pass filter over 400 nm (1250 ~ 1650 nm) wavelength range," OECC 2006 conference, Kaohsiung, Taiwan, 6D4-1, Jul. 3-7, 2006.
4. **Kuei-Chu Hsu**, Chii-Chang Chen, and Yinchieh Lai, "Highly directional edge emission from a photonic-crystal waveguide structure," OECC 2006 conference, Kaohsiung, Taiwan, 6D4-2, Jul. 3-7, 2006.
5. Lih-Gen Sheu, **Kuei-Chu Hsu**, and Yinchieh Lai, "Common-Path Interferometer for Dispersion Measurement of Fiber Bragg Gratings", CLEO2006 conference, Long beach, USA, JThC74, May 20-25, 2006.
6. Nan-Kuang Chen, **Kuei-Chu Hsu**, Hsiang-Jung Chang, Sien Chi, and Yinchieh Lai, "Tunable Er3+/Yb3+ codoped fiber amplifiers covering *S*- and *C*-Bands (1460 ~ 1580 nm) based on discrete fundamental-mode cutoff", OFC 2006 conference, Anaheim, USA, OThJ5, Mar. 5-10, 2006.
7. **Kuei-Chu Hsu**, Shu-Hui Chang, Kai-Ping Chuang, Yinchieh Lai, and Lih-Gen Sheu, "Nonlinear Photosensitive Effect on Refractive Index Profile and Spectral Response of Fiber Bragg Grating", OPT2005 conference, Tainan, Taiwan, B-SA-III 9-4, Dec 10-11, 2005.
8. **Kuei-Chu Hsu**, Lih-Gen Sheu, and Yinchieh Lai, "Fabrication of Fiber Bragg Gratings by Sequential UV-Writing with Real-Time Interferometric Side-Diffraction Position Monitoring", ECOC2005 conference, Glasgow, UK, We4.P.132, Sep 25-29, 2005.
9. **Kuei-Chu Hsu**, Shu-Hui Chang, Kai-Ping Chuang, Yinchieh Lai, and Lih-Gen Sheu, "Improved fiber Bragg grating step-scan exposure by interferometric side-diffraction position monitoring technique with reference fiber grating", OPT2004 conference, Taoyuan, Taiwan, B-SU-Ⅷ10-3, Dec 17-18, 2004.

## Patents

1. 徐桂珠，許立根，莊凱評，張淑惠，賴暎杰，"即時側向繞射監控光纖位置之布拉格光纖連續寫入方法，" (ROC patent no. 200641415, and USA patent pending).
2. 徐桂珠，許立根，項維巍，賴暎杰，"可用於窄頻濾波器之光纖光柵製作方法，" (ROC patent no. I282450).